



**HAL**  
open science

## Differential distribution of tight junction proteins suggests a role for tanycytes in blood-hypothalamus barrier regulation in the adult mouse brain.

Amandine Mullier, Sébastien G. Bouret, Vincent Prevot, Bénédicte Dehouck

### ► To cite this version:

Amandine Mullier, Sébastien G. Bouret, Vincent Prevot, Bénédicte Dehouck. Differential distribution of tight junction proteins suggests a role for tanycytes in blood-hypothalamus barrier regulation in the adult mouse brain.: Tanycytes at the blood-hypothalamus interface. *Journal of Comparative Neurology*, 2010, 518 (7), pp.943-62. 10.1002/cne.22273 . inserm-00487090

**HAL Id: inserm-00487090**

**<https://inserm.hal.science/inserm-00487090>**

Submitted on 27 May 2010

**HAL** is a multi-disciplinary open access archive for the deposit and dissemination of scientific research documents, whether they are published or not. The documents may come from teaching and research institutions in France or abroad, or from public or private research centers.

L'archive ouverte pluridisciplinaire **HAL**, est destinée au dépôt et à la diffusion de documents scientifiques de niveau recherche, publiés ou non, émanant des établissements d'enseignement et de recherche français ou étrangers, des laboratoires publics ou privés.

**Differential Distribution of Tight Junction Proteins Suggests  
a Role for Tanycytes in Blood-Hypothalamus Barrier  
Regulation in the Adult Mouse Brain**

Journal:	<i>The Journal of Comparative Neurology</i>
Manuscript ID:	JCN-09-0237.R4
Wiley - Manuscript type:	Research Article
Keywords:	ependymocytes, arcuate nucleus , hypothalamus, occludin, immunohistochemistry, mouse



Review

Submission: October 27, 2009

# Differential Distribution of Tight Junction Proteins Suggests a Role for Tanycytes in Blood-Hypothalamus Barrier Regulation in the Adult Mouse Brain

Amandine Mullier<sup>1,2</sup>, Sebastien G. Bouret<sup>1,2,3</sup>, Vincent Prevot<sup>1,2\*</sup> and Bénédicte Dehouck<sup>1,2</sup>

<sup>1</sup>Inserm, Jean-Pierre Aubert Research Center, Development and plasticity of the postnatal brain, U837, Lille Cedex, 59045, France

<sup>2</sup>Univ Lille Nord de France, Faculté de Médecine, Institut de médecine prédictive et recherche thérapeutique, place de Verdun, 59046 Lille Cedex, France

<sup>3</sup>The Saban Research Institute, Neuroscience Program, Children's Hospital of Los Angeles, University of Southern California, Los Angeles, California 90027, USA

**Abbreviated title:** Tanycytes at the blood-hypothalamus interface

**Key Words:** Ependymocytes, occludin, ZO-1, claudin, arcuate nucleus of the hypothalamus, immunohistochemistry

**\*Correspondence to:** Vincent Prevot, Inserm U837, Bâtiment Biserte, Place de Verdun, 59045 Lille Cedex, France. Phone: +33 320-62-20-64. E-mail: vincent.prevot@inserm.fr

**Grant support:** This work was supported by the NEUROBESE International Associated Laboratory (INSERM, SABAN, University of Lille2, to VP and SGB), the “Centre National de la Recherche Scientifique” (CNRS, to SGB), the “Agence Nationale de la Recherche” (ANR, to VP -GLIODIABESITY- and SGB -PROGRALEP-), the “Fondation pour la Recherche Médicale” (Equipe FRM to VP). AM was a Ph.D. student supported by a fellowship from the French “Ministère délégué à la Recherche et aux Nouvelles Technologies”.

**ABSTRACT**

The median eminence is one of the seven so-called circumventricular organs. It is located in the basal hypothalamus, ventral to the third ventricle and adjacent to the arcuate nucleus. This structure characteristically contains a rich capillary plexus and features a fenestrated endothelium, making it a direct target of blood-borne molecules. The median eminence also contains highly specialized ependymal cells called tanycytes which line the floor of the third ventricle. It has been hypothesized that one of the functions of these cells is to create a barrier that prevents substances in the portal capillary spaces from entering the brain. In this paper, we report on our use of immunohistochemistry to study the expression of tight junction proteins in the cells that compose the median eminence in adult mice. Our results indicate that tanycytes of the median eminence express occludin, ZO-1, and claudin 1 and 5, but not claudin 3. Remarkably, these molecules are organized as a continuous belt around the cell bodies of the tanycytes that line the ventral part of the third ventricle. In contrast, the tanycytes at the periphery of the arcuate nucleus do not express claudin 1 and instead exhibit a disorganized expression pattern of occludin, ZO-1 and claudin 5. Consistent with these observations, permeability studies using peripheral or central injections of Evans blue dye show that only the tanycytes of the median eminence are joined at their apices by functional tight junctions, whereas tanycytes located at the level of the arcuate nucleus form a permeable layer. In conclusion, this study reveals a unique expression pattern of tight junction proteins in hypothalamic tanycytes, which yields new insights into their barrier properties.

## INTRODUCTION

Tight junctions are the structural component of barriers in epithelial and endothelial sheets that control exchanges between two adjacent compositionally distinct compartments. They consist of molecular complexes that mediate the adhesion between adjacent cells while preventing the free passage of ions and molecules through the paracellular pathway. Tight junction proteins also play an important role in the establishment and maintenance of cell apico-basal polarity by restricting the diffusion of apical and basolateral membrane components. This polarity provides the necessary spatial cues for substances to be transported in a specific direction along the apico-basal axis (Cerejido et al., 1998; Shin et al., 2006). Structurally, tight junctions are comprised of transmembrane and membrane-associated proteins that are believed to assemble into stable complexes. *Zonula occludens-1* (ZO-1) and occludin were the first identified constitutive tight junction proteins (Furuse et al., 1993; Stevenson and Keon, 1998). These proteins are present in all cell layers that display barrier properties. More recently, scientists have discovered a family of transmembrane proteins designated the claudins. This family consists of at least 24 members, each of which exhibits both organ and tissue-specific distribution patterns (Morita et al., 1999).

In the central nervous system, tight junctions play a crucial role in the formation and maintenance of the blood-brain barrier. This barrier allows for the separation of internal environments between the blood and brain parenchyma compartments. However, there are discrete periventricular areas, known as the circumventricular organs, in which the brain endothelium is fenestrated. Several authors have noted that in these regions, the tight junction protein ZO-1 is expressed by ependymal as opposed to endothelial cells (Petrov et al., 1994; Smith and Shine, 1992), suggesting that the barrier has been shifted in these structures from the vascular to the ventricular side. The median eminence of the hypothalamus is one such circumventricular organ. Typically, the median eminence contains a rich capillary plexus and

a fenestrated endothelium (Schulz and Engelhardt, 2005). It also contains tanycytes that constitute the specialized ependymoglial cellular sheet that lines the floor and the basolateral walls of the third ventricle. A dominant feature of tanycytes is their marked polarization: tanycyte cell bodies are located in the ventral border of the third ventricle, but they also send processes to the vascular walls, where they make contact through “end feet” specializations (Ojeda et al., 2008; Prevot, 2002; Rutzel and Schiebler, 1980). Experimental evidence suggests that tanycytes are capable of transporting macromolecules between the blood and cerebrospinal fluid compartments via transcytosis (Fernandez-Galaz et al., 1996; Nakai and Naito, 1975; Peruzzo et al., 2004). The tanycytic cellular sheet lining the third ventricle is not composed of a homogenous cell population; four different types of tanycytes have been described based on their location, morphology, cytochemistry, ultrastructure and function (Akmayev and Fidelina, 1976; Akmayev et al., 1973; Akmayev and Popov, 1977; Rodriguez et al., 2005; Rodriguez et al., 1979).

Previous electron microscopic studies have mentioned the existence of tight junction complexes between tanycytes in the tuberal region of the hypothalamus based on morphological criteria (Brightman and Reese, 1969; Flament-Durand and Brion, 1985). Nevertheless, relatively little is known about the exact molecular nature of these putative tanycytic tight junction complexes. Moreover, there is still debate in the literature regarding the barrier properties of the ependymal sheet in this hypothalamic region (Brightman et al., 1975; Peruzzo et al., 2000).

Taking advantage of recent advances in the identification of the molecular components of tight junctions (Matter and Balda, 2003; Tsukita et al., 2001), our present study used immunohistochemistry to examine the differential spatial expression of tight junction proteins in ependymal cells of the tuberal region of the hypothalamus of adult mice. In addition, we used intravenous and intracerebroventricular injections of Evans blue dye to determine

whether distinct tight junction protein expression patterns at the ventricular wall of the third ventricle may be accompanied by localized differences in diffusion barriers.

For Peer Review

## **MATERIALS AND METHODS**

### **Animals and tissue preparation**

Fifteen male C57Black6 mice (Charles River, France) were used in this study. All experiments were carried out in accordance with the European Communities Council Directive of November 24th, 1986 (86/609/EEC) and the experimental protocols were approved by the local institutional research animal committee. Animals were maintained on a controlled light cycle (14 hours on / 10 hours off) and provided with food and water ad libitum. The animals were anesthetized with an intraperitoneal (i.p.) injection of chloral hydrate (8%; 350 mg/kg) and were perfused transcardially with 0.9% saline. The brains were quickly removed, embedded in ice-cold OCT (Optimal Cutting Temperature embedding medium, Tissue-Tek®, Sakura, France, Villeneuve d'Ascq), frozen in isopentane (-55°C) and stored at -80°C until sectioning. Using a cryostat, 20- $\mu$ m serial frozen sections were cut and collected on chrome-alum-gelatin-coated slides. Slide-mounted sections were fixed by immersion for either 1 minute at -20°C in methanol/acetone (vol/vol) for most immunostaining or for 10 minutes at 4°C in 2% paraformaldehyde for the detection of detyrosinated tubulin.

### **Antibody characterization**

All primary antibodies used are listed in table 1.

The occludin antiserum stained the expected band of 65 kD molecular weight on Western blots of mouse brain (Beauchesne et al., 2009; Koedel et al., 2002), and stained a pattern of membrane-associated structures in endothelial cells (Fig.4) that is identical with previous reports (Hirase et al., 1997).

The Zonula Occludens-1 (ZO-1) antiserum stained the expected band of 225 kD molecular weight on Western blots of mouse brain (Beauchesne et al., 2009; Stamatovic et al., 2005), and produced a pattern of staining in endothelial cells (Fig. 3A) and choroids plexus (data not shown) similar to that described elsewhere in the literature (Smith and Shine, 1992; Wolburg et al., 2001).

The claudin 1 antiserum had been previously characterized for immunocytochemical use by others in claudin 1 knockout mice (Furuse et al., 2002), and stained apical membrane-associated structures that exhibit the classical morphology of tight junction protein complexes (Fig. 10) that is identical with previous reports (Wolburg et al., 2001).

The claudin 3 antiserum had been previously shown to stain endothelial tight junctions in both human and mouse CNS (Wolburg et al., 2003), and stains capillary-associated structures that exhibit the classical morphology of the tight junction protein complexes seen in blood brain barrier capillaries (Fig. 9).

The claudin 5 antiserum stained the expected band of 22 kD molecular weight on Western blots of mouse brain (McColl et al., 2008; Stamatovic et al., 2005), and stained apical membrane-associated structures that exhibit the classical morphology of tight junction protein complexes (Fig. 8) that is identical with previous reports (Norsted et al., 2008). In addition, no staining was seen in mice in which the claudin 5 gene had been deleted (Nitta et al., 2003).

The detyrosinated tubulin antiserum (Gundersen et al., 1984) was shown to stain microtubules in neural tissue (Paturle-Lafanechere et al., 1994), and primary cilia *in vitro* (Gundersen and Bulinski, 1986).

The vimentin antiserum produced a pattern of staining similar to that described elsewhere by others (Kameda et al., 2003; Prevot, 2002; Sanchez et al., 2009) (Fig.1).

The von Willebrand factor antiserum produced a pattern of staining in vascular endothelial cells in the mouse CNS (Fig. 2) similar to that described elsewhere in the literature (Alliot et al., 1999).

The MECA 32 antiserum (Leppink et al., 1989) was raised against a mouse endothelial cell surface antigen as described previously by others (Streeter et al., 1988). This antibody has been shown to selectively recognize fenestrated capillaries in the circumventricular organs and the choroid plexus (Fig. 2) (Hallmann et al., 1995; Schulz and Engelhardt, 2005). It was a generous gift from Professor Britta Engelhardt (Switzerland).

### **Immunohistochemistry**

For dual-label immunofluorescence experiments, sections were rinsed 4 times in 0.1M phosphate buffer saline (PBS) (pH 7.4) and blocked for 1h using blocking solution (PBS containing 4% normal goat serum and 0.3% Triton X-100) at 4°C. Sections were incubated overnight at 4°C with primary antibodies diluted in blocking solution. The sections were then subjected to 4 washes in 0.1 M PBS and were incubated for 1h at room temperature with a mix of secondary Alexa Fluor-conjugated antibodies (1:500 dilution; all purchased from Molecular Probes, Invitrogen, San Diego, CA) in the blocking solution. The sections were rinsed 4 times in 0.1 M PBS. A nuclear counterstaining operation was performed by incubating the sections for 1 min in Hoechst (1:1,000 dilution; Molecular Probes, Invitrogen) diluted in 0.1 M PBS. Finally, sections were washed 4 times in 0.1 M phosphate buffer and coverslipped using Permafluor® (ThermoFisher, Illkirch, France). The slides were stored at 4°C until analysis. A special procedure was used to visualize the claudin 3 and 5 content. Antigen retrieval was performed using a microwave before the blocking step. Briefly, slides were incubated with 0.01 M citrate buffer (pH 6.0) and subjected to microwave irradiation (800W, 4 min then 400W, 2x5min) before the blocking step.

For triple-labeling studies, anti-vimentin antibodies were visualized using a goat anti-chicken biotin-conjugated antibody (1:500 dilution, 1h at room temperature; Vector Laboratories, Burlingame, CA) and AMCA-conjugated streptavidin (1:500 dilution, 1h at room temperature; Vector Laboratories).

### **Evans blue injection procedure**

Evans blue is a dye with high affinity for serum albumin, commonly used to assess the permeability of the blood-brain barrier (Hawkins and Egleton, 2006; Uyama et al., 1988). Adult male mice were subjected to either intravenous (i.v.) (n = 3) or intracerebroventricular (i.c.v., n = 3) injections of sterile 1% Evans blue (Sigma) in 0.9% saline, respectively. Animals injected into the tail vein with Evans blue (50  $\mu$ L) were killed by decapitation 20 minutes post-injection. For i.c.v. injections, mice were placed in a stereotactic frame (Kopf® Instruments, California) under anesthesia (0.06 g/kg ketamine and 0.01 g/kg xylazine, both i.p.), and a burr hole was drilled 1 mm lateral to the Bregma and 0.3 mm posterior to the Bregma, according to a mouse brain atlas (Paxinos & Franklin, 2001). A 10  $\mu$ L Hamilton syringe was slowly inserted into the left lateral ventricle (2.5 mm deep relative to the dura). The cisterna magna was exposed to the atmosphere and 2  $\mu$ L of Evans blue was immediately injected into the left lateral ventricle using an infusion pump (KD Scientific, Holliston, MA) over 1 min. The needle of the Hamilton syringe was removed 1 min after the injection ended and the mice were killed by decapitation.

Brains of the injected mice were quickly removed, frozen in O.C.T. and stored at -80°C until use. Serial frozen sections (20  $\mu$ m) were cut on a cryostat and collected on gelatin-coated glass slides. The Evans blue staining was directly visualized and imaged with a fluorescent microscope. Slide-mounted sections were then fixed in methanol/acetone (vol/vol) at -20°C for 1 minute, dried at room temperature and processed immediately for immunohistochemistry analyses as described above.

### Microscopic analysis

Sections were analyzed using an Axio Imager.Z1 ApoTome microscope (Zeiss, Germany), equipped with a motorized stage and an AxioCam MRm camera (Zeiss, Germany). Specific filter cubes were used for the visualization of green (EX: 475/40 nm, DM: 500 nm, BA: 530/50 nm), red (EX: 550/25 nm, DM: 570 nm, BA: 605/70 nm), and UV (bisbenzimidide) or AMCA (amino-methyl-coumarin-acetate) fluorescence (EX: 365 nm, DM: 395 nm, BA: 445/50 nm).

To create photomontages, single-plane images were captured using the MosaiX module of the AxioVision 4.6 system (Zeiss, Germany) and a Zeiss 20X objective (N.A. 0.8) for each fluorophore sequentially. Adobe Photoshop (Adobe Systems, San Jose, CA) was then used to process, by applying adjustments for brightness and contrast, and merge the photomontages.

High magnification microphotographs represent maximal intensity projections derived from 20-25 triple-apoTome images collected using the z-stack module of the AxioVision 4.6 system and a Zeiss 63X oil immersion objective (N.A. 1.4). All images were captured in a stepwise fashion over a defined z-focus range corresponding to all visible staining within the section and consistent with the optimum step size for the corresponding objective and the wavelength ( $\lambda=500$  nm).

Confocal laser scanning microscopy was used to confirm the spatial organization and distribution of all tight junction proteins. Sections were examined with a Leica SP2 upright confocal laser scanning microscope (DM RAX-UV) equipped with the Acousto-Optical Beam Splitter (AOBS) and using a 100X, N.A. 1.4, oil immersion objective (Leica Microsystems, Rueil-Malmaison, France). DAPI was excited at 405 nm and observed from 420 to 495 nm, Alexa 488 was excited at 488 nm and observed from 495 to 580 nm, Alexa 568 was excited at 594 nm and observed from 599 to 680 nm. The selection of the spectral emission window for each fluorophore was determined through  $\lambda$  scan analysis of single stained membrane

fragments. The gain and offset for each photomultiplier were adjusted to optimize nucleic acid, tight junction protein and vimentin detection events. Images of the confocal laser scanning microscopy observations (1024 by 1024 pixels) were acquired sequentially, between stacks, to eliminate spectral crosstalk from the data. The frequency was set to 200 Hz and the signal/noise ratio was enhanced through frame averaging. Overlays and maximum projections of the z-stack files were performed post-acquisition by using the Leica Confocal Software to obtain the presented images. Original z-stack Leica files were imported into the Imaris 6.0 software package (Bitplane AG, Zürich, Switzerland) to perform 3D modeling.

### **Distributions of the different ependymogial cell types in the tuberal region of the hypothalamus**

Cell counts were assessed 1.9 mm posterior to the Bregma (Paxinos & Franklin, 2001). Single-plane images were acquired from two 20- $\mu$ m-thick frontal sections separated by 40 $\mu$ m, using the ApoTome technology. Different ependymogial cell types were identified according to anatomical criteria, vimentin immunoreactivity, and their pattern of occludin expression (honeycomb or unorganized). For quantification purposes, the wall of the third ventricle was divided into four parts depending on the hypothalamic structure adjacent to the ventricle: the median eminence (ME), the arcuate nucleus of the hypothalamus (ARH), the ventromedial nucleus of the hypothalamus (VMH) and the dorsomedial nucleus of the hypothalamus (DMH) respectively. For each image and subdivision, we counted the total number of cell nuclei lining the third ventricle. Cells of each different ependymogial cell type were counted. Using this method, each cell was counted only once and was thus categorized under a single group. The results from our analysis of two sections per animal were combined and the percentages of cells belonging to each category were calculated. Quantifications were performed using 3 animals. To avoid observer bias, quantifications were repeated by an independent investigator who was unaware of the respective experimental conditions.

## Statistics

The differences between several groups were analyzed by one-way ANOVA followed by the Student-Newman-Keuls multiple comparison test for unequal replications. Statistical significance was accepted if  $p < 0.05$ . To compare percentages, groups were subjected to arc-sine transformation prior to statistical analysis to convert them from a binomial to a normal distribution.

For Peer Review

## RESULTS

First, we briefly assessed the normal anatomical distribution and morphology of vimentin-positive cells and their association with brain capillaries. Vimentin immunoreactivity was distributed throughout the cells lining the third ventricle, exhibiting a different expression pattern in tanycytes located in the ventral region of the ventricle as compared with that seen in the “typical” ependymal cells (Knowles, 1972; Mathew, 2008) that are mainly located in the dorsal third of the ventricle (red, Fig 1). The tanycytes exhibited intense apical vimentin immunostaining and extended long and slender vimentin-positive processes towards the nervous parenchyma (Fig. 1A, D, E). Of note, the “typical” ependymal cells that are known to be devoid of process, typically displayed intense vimentin immunostaining restricted to a prominent, round and centrally located nucleus (Fig. 1A-C). Unlike the tanycytes, these cuboidal ependymal cells exhibit tufts of cilia on their luminal (apical) surfaces. This feature was assessed using detyrosinated-tubulin immunoreactivity (Fig. 1A-D). The first ciliated ependymal cells appeared dorsal to the arcuate nucleus in the portion of the ventricular wall adjacent to the ventromedial nucleus (VMH). Ciliated ependymal cells became more abundant in the dorsal portion of the third ventricle, at the level of the dorsomedial nucleus (DMH), while the population of tanycytes gradually declined until only ciliated ependymal cells were present. Demonstrating the relationship of tanycytes with brain capillaries, Figure 2 shows that vimentin immunoreactive tanycytes bordering the floor of the third ventricle were in direct contact with the MECA 32-immunoreactive fenestrated capillaries (blue, Fig. 2B,D) at the external zone of the median eminence (ME). By contrast, dorsolateral tanycytes were in contact with MECA 32-immunonegative, von Willebrand factor-immunopositive brain capillaries (Fig. 2B, C). These observations thus suggest that there are at least two different populations of tanycytes that can be distinguished according to the type of blood vessels they interact with in the tuberal region of the hypothalamus.

### **Co-distribution of ZO-1 and occludin immunoreactivities in ependymogial cells lining the third ventricle within the tuberal region of the hypothalamus**

The presence of tight junction protein immunoreactivity in the wall of the third ventricle at the median eminence has not been fully investigated to date. Accordingly, we analyzed the distribution of ZO-1 and occludin immunostaining as these are intracellular and transmembrane proteins, respectively, which are known to physically interact at tight junction complexes (Tsukita et al., 2001). As expected, ZO-1 (Fig. 3A,B) and occludin (Fig. 4A,B) immunoreactivities were recorded in brain capillaries throughout the nervous tissue. Predominant staining of ZO-1 and occludin in choroid plexus epithelium was observed, also as expected (data not shown). Importantly, ZO-1-and occludin- immunostaining was also identified close to the ventricular surface (Fig. 3B, 4B). Greatly magnified images revealed that ZO-1 and occludin expression was closely associated with ependymocytes, with distinct expression patterns among the different ependymal cell types. In tanycytes located at the levels of the median eminence, ZO-1 and occludin immunoreactivities were organized around the cell bodies in a continuous belt, giving rise to a honeycomb-like shape (Fig. 3F,G, 4F,G). In contrast, tanycytes lining the region of the ventricle adjacent to the ARH exhibited a diffuse pattern of ZO-1 and occludin immunoreactivity in the apical region of the cells (Fig. 3E, 4E). Similar to tanycytes of the median eminence, an organized pattern of ZO-1 and occludin labeling was observed in ependymal cells dorsal to the ARH (Fig. 3C, 4C).

Confocal analysis (Fig. 5A,C) and 3-D reconstruction (Fig. 5B,D) of 20- $\mu$ m-thick sections suggested that the diffuse apical occludin staining found in ARH tanycytes was not an orientation-related or tangential sectioning artifact. To further confirm that the unorganized pattern of tight-junction protein immunoreactivity observed in ARH tanycytes was not due to the potential orthogonal orientation of these cells in the section plane, we studied occludin immunoreactivity in sagittal sections. Figure 6 shows that in contrast to median eminence

tanycytes (Fig. 6A,C) and typical ependymocytes (Fig. 6A,B), both of which display honeycomb-like occludin immunoreactivity, dorsal tanycytes exhibit an unorganized pattern of occludin labeling (Fig. 6A,D).

Remarkably, a combination of cells harboring either organized or unorganized patterns of ZO-1 (Fig 3D) and occludin (Fig. 4D) was found in the region of the ventricular wall adjacent to the VMH. To determine the identities of these cells, we performed quantitative analyses based on morphological criteria. Each individual cell was categorized according to its pattern of vimentin and tight junction protein immunoreactivity. The results in Figure 7 indicate that the cells in the ventricular wall apposed to the VMH that exhibited a honeycomb pattern of occludin expression were cuboidal ependymal cells, while the tanycytes exhibited the typical diffuse occludin expression. Within the median eminence,  $79.71 \pm 3.06 \%$  of the cells on the ventricular surface were tanycytes harboring a honeycomb pattern of occludin expression (Fig. 7M). The proportion of these cells dropped dramatically at the ARH, VMH and DMH ( $< 20 \%$ ; one way ANOVA,  $p < 0.001$ ,  $n = 3$  animals). Conversely, the proportion of tanycytes exhibiting an unorganized pattern of occludin labeling was very low at the median eminence ( $9.25 \pm 1.22 \%$ ), increased noticeably at the ARH ( $79.28 \pm 4.37 \%$ ; one way ANOVA, median eminence *vs.* ARH,  $p < 0.05$ ), remained high at the VMH ( $57.08 \pm 14.71 \%$ ; one way ANOVA, median eminence *vs.* VMH,  $p < 0.05$ ) and fell back under  $10 \%$  at the DMH (one way ANOVA, ARH *vs.* DMH and VMH *vs.* DMH,  $p < 0.05$ ). In contrast, cuboidal ependymal cells, which were absent from the ventricular wall at the median eminence and the ARH, appeared at the VMH ( $16.67 \pm 8.82 \%$ ) and the abundance of these cells that show organized pattern of occludin immunoreactivity significantly increased at the DMH ( $66.98 \pm 6.08 \%$ ;  $p < 0.01$ ).

### **Localization of claudin 1, 3, 5 immunoreactivities in the tuberal region of the hypothalamus**

Because occludin and claudins are thought to assemble into heteropolymers to form tight junction intramembrane strands (Tsukita et al., 2001), we next sought to determine whether claudins may be expressed in the cells lining the ventricular wall of the third ventricle. We performed immunostaining for claudin 1, claudin 3, and claudin-5, all of which have previously been shown to be expressed in the central nervous system (Furuse et al., 2002; Nitta et al., 2003; Wolburg et al., 2003). Interestingly, these three tight junction integral membrane proteins exhibited very distinct patterns of distribution in the tuberal region of the hypothalamus. While claudin 5 immunolabeling exhibited an expression pattern very similar to that seen for occludin and ZO-1 (Fig. 8), claudin 3-immunostaining was only found in brain capillaries (Fig. 9) and claudin 1-immunoreactivity was restricted to the ventral part of the third ventricle wall (Fig. 10). Figure 10 demonstrates that claudin 1 immunoreactivity is concentrated in the most apical part of tanycytes of the median eminence, where it forms a honeycomb pattern. In contrast, arcuate tanycytes, cuboidal ependymal cells and brain capillaries were devoid of claudin 1 immunoreactivity.

### **Blood-hypothalamus and cerebrospinal fluid-hypothalamus interfaces in tanycytes of the median eminence**

To determine whether tight junction protein expression patterns reflect localized diffusion barriers, we used Evans blue dye. Mice were injected either into their tail vein or lateral ventricle with Evans blue dye as described in the Materials and Methods section. Intravenous injection of Evans blue resulted in the diffusion of the dye being restricted to the vascular bed of hypothalamic capillaries (arrow, Fig. 11A) and the median eminence (asterisks, Fig. 11A). Noticeably, the Evans blue dye bathing the median eminence did not spread into the neighboring hypothalamic structures, including the ARH (Fig. 11F). By

contrast, when injected into the lateral ventricle, the Evans blue dye diffused into the ARH while the median eminence remained dye-free (Fig. 11G, L). Intriguingly, the Evans blue dye that penetrated into the ARH did not spread to other hypothalamic structures such as the VMH and DMH (Fig. 11L).

For Peer Review

## DISCUSSION

In the present study, we used immunocytochemistry to systematically examine the distribution of tight junction proteins in the cells that line the ventricular wall of the third ventricle in the tuberal region of the hypothalamus. Our results reveal differential patterns of tight junction protein expression between different ependymoglial cell types and locations. The localization of these different patterns parallel the domains of the ventricular wall that exhibit distinct diffusion properties, as shown by central and peripheral injections of Evans blue dye. Our findings are consistent with the proposed role of median eminence tanycytes in regulating blood-hypothalamus exchanges by forming a cellular sheet that is impermeable to blood-borne molecules at the floor of the third ventricle. In contrast, arcuate tanycytes formed a permeable layer that allowed unrestrained diffusion of molecules between the cerebrospinal fluid and ARH compartments.

Others have established that in the CNS, diffusion barriers are built using tight junction complexes in which occludin, ZO-1, claudin 5, claudin 1 and claudin 3 play key functional roles (Furuse et al., 1993; Morita et al., 1999; Stevenson and Keon, 1998). The present study provides the first extensive characterization of tight junction protein expression patterns in the ventricular wall of the third ventricle. Our findings are summarized in Figure 12. The results indicate that the tanycytes of the median eminence display a honeycomb-like pattern of immunoreactivity for occludin, ZO-1, claudin 1 and claudin 5, but they do not express claudin 3. Rather, the latter molecule is readily and selectively detected in the capillaries of the blood-brain barrier (BBB), as confirmed previously by others (Wolburg et al., 2003). The cobblestone immunoreactivity pattern is typical of tight junction proteins (Tsukita and Furuse, 2002) and has been reported in the choroid plexus epithelium (Wolburg et al., 2001). In epithelial cells, tight junctions are indeed located at the most apical region of

lateral membranes, and are composed of sealing strands of integral proteins that hold adjacent plasma membranes together (Tsukita and Furuse, 2002; Tsukita et al., 2001). To function as a paracellular barrier, this belt-like anchoring junction should be continuous and should encircle each of the interacting cells in the sheet, thus giving rise to the typical honeycomb-staining pattern of junction associated proteins (Coisne et al., 2005; Wolburg et al., 2001). The fact that both central and peripheral injections of Evans blue dye do not diffuse through the cellular sheet that is formed by median eminence tanycytes convincingly demonstrates that these specialized ependymogial cells are joined at their apices by functional tight junctions. These results are consistent with the work of Brightman and Reese that visualized tight junction-like complexes in the median eminence using electron microscopy (Brightman and Reese, 1969). Besides, our study supplements the work of Petrov and coauthors, who demonstrated ZO-1 immunoreactivity in cells lining the ventricular walls and in median eminence tanycytes (Petrov et al., 1994; Smith and Shine, 1992), by reporting the expression of 3 additional proteins that are known to be associated with tight junction complexes; namely occludin, claudin 1 and claudin 5.

The present study also reveals that occludin, ZO-1, and claudin 5 immunoreactivities are abundantly detectable in the arcuate tanycytes and in the cuboidal ependymocytes that pave the dorsal third of the wall of the third ventricle. By contrast, claudin 1 is selectively expressed in the tanycytes of the median eminence. However, while the cuboidal ependymal cells displayed honeycomb-like staining patterns for tight junction proteins, the arcuate tanycytes intriguingly showed unorganized and diffuse apical expression patterns for occludin, ZO-1, and claudin 5. The latter results are in agreement with previous electron microscopic studies in rats in which they mentioned morphologically the existence of “incomplete ependymal tight junctions” facing towards the ARH (Brightman et al., 1975; Gotow and Hashimoto, 1981). Consistent with these observations, intracerebroventricular

injections of Evans blue demonstrated that the arcuate tanycyte layer was permeable to the dye, suggesting that uncontrolled exchanges of solutes may occur between the cerebrospinal fluid and the ARH compartments. On the other hand, central infusion of Evans blue did not penetrate the cellular sheet formed by cuboidal ependymal cells. These results stand in contrast to previous studies in which they used HRP as a tracer (Brightman and Reese, 1969) and upon intracerebroventricular injections showed its dispersal in all hypothalamic nuclei of the periventricular zone (ARH, VMH and DMH). In our present studies, diffusion of Evans blue originating from the cerebrospinal fluid is restricted to the ARH. The VMH and DMH are not flooded with the tracer, neither is the median eminence, thus confirming the existence of diffusion barriers between the ARH and both the median eminence and VMH described previously (Rethelyi, 1984). The nature of these diffusion barriers that reside into the parenchyma remains to be fully characterized (Rodriguez et al., 2005). Taken together, our results indicate that the assembly and regulation of tight junction complexes in ependymal cells in general, and in tanycytes in particular, differ between distinct domains of the wall of the third ventricle. Because median eminence tanycytes directly contact Evans blue permeable fenestrated capillaries while arcuate tanycytes contact Evans blue-impermeable blood-brain barrier capillaries, it is possible that the differences in tight junction protein organization and diffusion barrier permeability between these two tanycytic cell populations is related to this major distinguishing anatomical feature.

Although the distribution of tight junction proteins in the different domains of the third ventricular wall is obviously correlated with the Evans blue permeability of the paving cellular sheet, such a parallel is not apparent at the VMH transitional zone. At the interface between the cerebrospinal fluid and brain parenchyma compartments, exclusion of centrally-infused Evans blue dye from the VMH is not associated with an unambiguous honeycomb pattern distribution of tight junction proteins in ependymal cells. The tightness of the seal

created by ependymal cells may thus not be the sole mechanism involved in the restriction of exchanges between the cerebrospinal fluid and tissue compartments. Interestingly, the transitional zone at the VMH is where the first ciliated ependymal cells, which are totally absent at the ARH, are found. Beating of ependymal cilia sets in motion cerebrospinal fluid flow (Sawamoto et al., 2006) and may thus limit the exchanges between the cerebrospinal fluid compartment and the ependymal sheet at the surface of the third ventricle. This may contribute to the exclusion of ventricular Evans blue from the VMH. By contrast, the arcuate and median eminence tanycytes both lack cilia. Thus the cerebrospinal fluid flow at the floor of the third ventricle may be dramatically lower and diffusional exchanges between the cerebrospinal fluid and ARH compartments may be markedly facilitated. Interestingly, arcuate tanycytes have been previously shown to possess microvilli at their luminal surfaces (Brawer, 1972; Bruni et al., 1972) suggesting that this cell population may play an important role in sensing molecules in the cerebrospinal fluid. This population may also be actively involved in promoting exchanges between the cerebrospinal fluid and the brain compartments at the ARH.

The ARH is a critical component of the neural pathways that regulate energy balance, and therefore plays a key role in relaying blood-borne molecular signals. Research into this process has largely focused on the involvement of the ARH in relaying leptin signals to other parts of the hypothalamus (Elmqvist et al., 2005; Sawchenko, 1998). However, the mechanisms by which peripheral signals reach the ARH to mediate their central effects remain largely unknown, although several hypotheses refer to the presence of fenestrated capillaries at the ARH (Ciofi et al., 2006) and the existence of a weak BBB at the ARH (Norsted et al., 2008). The results of the present study strongly suggest that exchanges between the cerebrospinal fluid and the ARH milieu can be notably facilitated. It is tempting to speculate that one possible route for blood-borne molecules to target the ARH would be via

the cerebrospinal fluid. Transcytosis studies have substantiated a possible role for the tanycytes of the median eminence in conveying blood-borne molecules to the cerebrospinal fluid (Nakai and Naito, 1975), and conversely (Garcia-Segura et al., 1999; Peruzzo et al., 2004). Consistent with this hypothesis, our results indicate that the ventral tanycytes are highly polarized due to the presence of efficient tight junction complexes. Indeed, tight junctions are not only known to prevent the diffusion of solutes through the paracellular cleft, but they are also understood to be the principal structures contributing to cell polarity. In this role, they act as an intramembrane barrier to prevent the lateral diffusion of integral membrane proteins that localize to specific sites in the apical or basolateral regions of the cell (Cereijido et al., 1998; Shin et al., 2006).

To our knowledge this is the first detailed study of the differential spatial distribution of tight junction proteins in the tuberal region of the hypothalamus in the adult mouse. The results of our immunofluorescence studies, together with dye permeability experiments, provide detailed and additional information about the diffusion barriers between blood-brain, blood-cerebrospinal fluid and cerebrospinal fluid-brain compartments in this region of the CNS. These data identify the periventricular zone of the tuberal region of the hypothalamus, which contains the median eminence and ARH, as a key interface for blood-cerebrospinal fluid-brain exchanges, and also demonstrates that while fenestrated vessels in the median eminence allow the diffusion of blood-born molecules into the median eminence milieu, this “brain window” is restricted to the median eminence parenchyma. These data suggest a role for the median eminence tanycytes in controlling these barrier properties. Immunohistochemical results have also suggested that arcuate tanycytes are devoid of efficient tight junction complexes, thus confirming that the ependymal sheet lining the ARH is privileged as an interface for the exchange of molecules between the cerebrospinal fluid and brain parenchyma compartments. Overall, the results of our study support the hypothesis

that the median eminence acts as a putative route for peripheral molecules to specifically target the ARH.

For Peer Review

**OTHER ACKNOWLEDGEMENTS**

Confocal analyses were performed at the “Plate-forme régionale de recherche en imagerie cellulaire”, INSERM U413 - IFRMP 23, Université de Rouen, Mont-Saint-Aignan, France. The MECA 32 antibodies were kindly provided by Professor Britta Engelhardt (Switzerland).

**LITERATURE CITED**

- Akmayev IG, Fidelina OV. 1976. Morphological aspects of the hypothalamic-hypophyseal system. VI. The tanycytes: their relation to the sexual differentiation of the hypothalamus. An enzyme-histochemical study. *Cell Tissue Res* 173(3):407-416.
- Akmayev IG, Fidelina OV, Kabolova ZA, Popov AP, Schitkova TA. 1973. Morphological aspects of the hypothalamic-hypophyseal system. IV. Medial basal hypothalamus. An experimental morphological study. *Z Zellforsch Mikrosk Anat* 137(4):493-512.
- Akmayev IG, Popov AP. 1977. Morphological aspects of the hypothalamic-hypophyseal system. VII. The tanycytes: Their relation to the hypophyseal adrenocorticotrophic function. An ultrastructural study. *Cell Tissue Res* 180(2):263-282.
- Alliot F, Rutin J, Leenen PJ, Pessac B. 1999. Brain parenchyma vessels and the angiotensin system. *Brain Res* 830(1):101-112.
- Beauchesne E, Desjardins P, Hazell AS, Butterworth RF. 2009. Altered expression of tight junction proteins and matrix metalloproteinases in thiamine-deficient mouse brain. *Neurochem Int* 55(5):275-281.
- Brawer JR. 1972. The fine structure of the ependymal tanycytes at the level of the arcuate nucleus. *J Comp Neurol* 145(1):25-41.
- Brightman MW, Prescott L, Reese ST. 1975. Intercellular junctions of special ependyma. In: Knigge KM, Scott DE, Kobayashi H, Miura-shi, Ishii S, editors. *Brain-Endocrine Interaction II The Ventricular System*: Karger, Basel. p 146 - 165.
- Brightman MW, Reese TS. 1969. Junctions between intimately apposed cell membranes in the vertebrate brain. *J Cell Biol* 40(3):648-677.
- Bruni JE, Montemurro DG, Clattenburg RE, Singh RP. 1972. A scanning electron microscopic study of the ependymal surface of the third ventricle of the rabbit, rat, mouse and human brain. *Anat Rec* 174(4):407-420.
- Cereijido M, Valdes J, Shoshani L, Contreras RG. 1998. Role of tight junctions in establishing and maintaining cell polarity. *Annu Rev Physiol* 60:161-177.
- Ciofi P, Leroy D, Tramu G. 2006. Sexual dimorphism in the organization of the rat hypothalamic infundibular area. *Neuroscience* 141(4):1731-1745.
- Coisne C, Dehouck L, Faveeuw C, Delplace Y, Miller F, Landry C, Morissette C, Fenart L, Cecchelli R, Tremblay P, Dehouck B. 2005. Mouse syngenic in vitro blood-brain

- barrier model: a new tool to examine inflammatory events in cerebral endothelium. *Lab Invest* 85(6):734-746.
- Elmqvist JK, Coppari R, Balthasar N, Ichinose M, Lowell BB. 2005. Identifying hypothalamic pathways controlling food intake, body weight, and glucose homeostasis. *J Comp Neurol* 493(1):63-71.
- Fernandez-Galaz MC, Torres-Aleman I, Garcia-Segura LM. 1996. Endocrine-dependent accumulation of IGF-I by hypothalamic glia. *Neuroreport* 8(1):373-377.
- Flament-Durand J, Brion JP. 1985. Tanycytes: morphology and functions: a review. *Int Rev Cytol* 96:121-155.
- Furuse M, Hata M, Furuse K, Yoshida Y, Haratake A, Sugitani Y, Noda T, Kubo A, Tsukita S. 2002. Claudin-based tight junctions are crucial for the mammalian epidermal barrier: a lesson from claudin-1-deficient mice. *J Cell Biol* 156(6):1099-1111.
- Furuse M, Hirase T, Itoh M, Nagafuchi A, Yonemura S, Tsukita S, Tsukita S. 1993. Occludin: a novel integral membrane protein localizing at tight junctions. *J Cell Biol* 123(6 Pt 2):1777-1788.
- Garcia-Segura LM, Naftolin F, Hutchison JB, Azcoitia I, Chowen JA. 1999. Role of astroglia in estrogen regulation of synaptic plasticity and brain repair. *J Neurobiol* 40(4):574-584.
- Gotow T, Hashimoto PH. 1981. Graded differences in tightness of ependymal intercellular junctions within and in the vicinity of the rat median eminence. *J Ultrastruct Res* 76(3):293-311.
- Gundersen GG, Bulinski JC. 1986. Microtubule arrays in differentiated cells contain elevated levels of a post-translationally modified form of tubulin. *Eur J Cell Biol* 42(2):288-294.
- Gundersen GG, Kalnoski MH, Bulinski JC. 1984. Distinct populations of microtubules: tyrosinated and nontyrosinated alpha tubulin are distributed differently in vivo. *Cell* 38(3):779-789.
- Hallmann R, Mayer DN, Berg EL, Broermann R, Butcher EC. 1995. Novel mouse endothelial cell surface marker is suppressed during differentiation of the blood brain barrier. *Dev Dyn* 202(4):325-332.
- Hawkins BT, Egleton RD. 2006. Fluorescence imaging of blood-brain barrier disruption. *J Neurosci Methods* 151(2):262-267.
- Hirase T, Staddon JM, Saitou M, Ando-Akatsuka Y, Itoh M, Furuse M, Fujimoto K, Tsukita S, Rubin LL. 1997. Occludin as a possible determinant of tight junction permeability in endothelial cells. *J Cell Sci* 110 ( Pt 14):1603-1613.
- Kameda Y, Arai Y, Nishimaki T. 2003. Ultrastructural localization of vimentin immunoreactivity and gene expression in tanycytes and their alterations in hamsters kept under different photoperiods. *Cell Tissue Res* 314(2):251-262.
- Knowles F. 1972. Ependyma of the third ventricle in relation to pituitary function. *Prog Brain Res* 38:255-270.
- Koedel U, Winkler F, Angele B, Fontana A, Pfister HW. 2002. Meningitis-associated central nervous system complications are mediated by the activation of poly(ADP-ribose) polymerase. *J Cereb Blood Flow Metab* 22(1):39-49.

- Leppink DM, Bishop DK, Sedmak DD, Henry ML, Ferguson RM, Streeter PR, Butcher EC, Orosz CG. 1989. Inducible expression of an endothelial cell antigen on murine myocardial vasculature in association with interstitial cellular infiltration. *Transplantation* 48(5):874-877.
- Mathew TC. 2008. Regional analysis of the ependyma of the third ventricle of rat by light and electron microscopy. *Anat Histol Embryol* 37(1):9-18.
- Matter K, Balda MS. 2003. Holey barrier: claudins and the regulation of brain endothelial permeability. *J Cell Biol* 161(3):459-460.
- McColl BW, Rothwell NJ, Allan SM. 2008. Systemic inflammation alters the kinetics of cerebrovascular tight junction disruption after experimental stroke in mice. *J Neurosci* 28(38):9451-9462.
- Morita K, Furuse M, Fujimoto K, Tsukita S. 1999. Claudin multigene family encoding four-transmembrane domain protein components of tight junction strands. *Proc Natl Acad Sci U S A* 96(2):511-516.
- Nakai Y, Naito N. 1975. Uptake and bidirectional transport of peroxidase injected into the blood and cerebrospinal fluid by ependymal cells of the median eminence. In: Knigge KM, Scott DE, Kobayashi H, Miura-shi, Ishii S, editors. *Brain-Endocrine Interaction II The ventricular system*: Karger, Basel. p 94 - 108.
- Nitta T, Hata M, Gotoh S, Seo Y, Sasaki H, Hashimoto N, Furuse M, Tsukita S. 2003. Size-selective loosening of the blood-brain barrier in claudin-5-deficient mice. *J Cell Biol* 161(3):653-660.
- Norsted E, Gomuc B, Meister B. 2008. Protein components of the blood-brain barrier (BBB) in the mediobasal hypothalamus. *J Chem Neuroanat* 36(2):107-121.
- Ojeda SR, Lomniczi A, Sandau US. 2008. Glial-gonadotrophin hormone (GnRH) neurone interactions in the median eminence and the control of GnRH secretion. *J Neuroendocrinol* 20(6):732-742.
- Paturle-Lafanechere L, Manier M, Trigault N, Pirollet F, Mazarguil H, Job D. 1994. Accumulation of delta 2-tubulin, a major tubulin variant that cannot be tyrosinated, in neuronal tissues and in stable microtubule assemblies. *J Cell Sci* 107 ( Pt 6):1529-1543.
- Peruzzo B, Pastor FE, Blazquez JL, Amat P, Rodriguez EM. 2004. Polarized endocytosis and transcytosis in the hypothalamic tanycytes of the rat. *Cell Tissue Res* 317(2):147-164.
- Peruzzo B, Pastor FE, Blazquez JL, Schobitz K, Pelaez B, Amat P, Rodriguez EM. 2000. A second look at the barriers of the medial basal hypothalamus. *Exp Brain Res* 132(1):10-26.
- Petrov T, Howarth AG, Krukoff TL, Stevenson BR. 1994. Distribution of the tight junction-associated protein ZO-1 in circumventricular organs of the CNS. *Brain Res Mol Brain Res* 21(3-4):235-246.
- Prevot V. 2002. Glial-neuronal-endothelial interactions are involved in the control of GnRH secretion. *J Neuroendocrinol* 14(3):247-255.
- Rethelyi M. 1984. Diffusional barrier around the hypothalamic arcuate nucleus in the rat. *Brain Res* 307(1-2):355-358.

- Rodriguez EM, Blazquez JL, Pastor FE, Pelaez B, Pena P, Peruzzo B, Amat P. 2005. Hypothalamic tanycytes: a key component of brain-endocrine interaction. *Int Rev Cytol* 247:89-164.
- Rodriguez EM, Gonzalez CB, Delannoy L. 1979. Cellular organization of the lateral and postinfundibular regions of the median eminence in the rat. *Cell Tissue Res* 201(3):377-408.
- Rutzel H, Schiebler TH. 1980. Prenatal and early postnatal development of the glial cells in the median eminence of the rat. *Cell Tissue Res* 211(1):117-137.
- Sanchez E, Vargas MA, Singru PS, Pascual I, Romero F, Fekete C, Charli JL, Lechan RM. 2009. Tanycyte pyroglutamyl peptidase II contributes to regulation of the hypothalamic-pituitary-thyroid axis through glial-axonal associations in the median eminence. *Endocrinology* 150(5):2283-2291.
- Sawamoto K, Wichterle H, Gonzalez-Perez O, Cholfin JA, Yamada M, Spassky N, Murcia NS, Garcia-Verdugo JM, Marin O, Rubenstein JL, Tessier-Lavigne M, Okano H, Alvarez-Buylla A. 2006. New neurons follow the flow of cerebrospinal fluid in the adult brain. *Science* 311(5761):629-632.
- Sawchenko PE. 1998. Toward a new neurobiology of energy balance, appetite, and obesity: the anatomists weigh in. *J Comp Neurol* 402(4):435-441.
- Schulz M, Engelhardt B. 2005. The circumventricular organs participate in the immunopathogenesis of experimental autoimmune encephalomyelitis. *Cerebrospinal Fluid Res* 2:8.
- Shin K, Fogg VC, Margolis B. 2006. Tight junctions and cell polarity. *Annu Rev Cell Dev Biol* 22:207-235.
- Smith GM, Shine HD. 1992. Immunofluorescent labeling of tight junctions in the rat brain and spinal cord. *Int J Dev Neurosci* 10(5):387-392.
- Stamatovic SM, Shakuji P, Keep RF, Moore BB, Kunkel SL, Van Rooijen N, Andjelkovic AV. 2005. Monocyte chemoattractant protein-1 regulation of blood-brain barrier permeability. *J Cereb Blood Flow Metab* 25(5):593-606.
- Stevenson BR, Keon BH. 1998. The tight junction: morphology to molecules. *Annu Rev Cell Dev Biol* 14:89-109.
- Streeter PR, Rouse BT, Butcher EC. 1988. Immunohistologic and functional characterization of a vascular addressin involved in lymphocyte homing into peripheral lymph nodes. *J Cell Biol* 107(5):1853-1862.
- Tsukita S, Furuse M. 2002. Claudin-based barrier in simple and stratified cellular sheets. *Curr Opin Cell Biol* 14(5):531-536.
- Tsukita S, Furuse M, Itoh M. 2001. Multifunctional strands in tight junctions. *Nat Rev Mol Cell Biol* 2(4):285-293.
- Uyama O, Okamura N, Yanase M, Narita M, Kawabata K, Sugita M. 1988. Quantitative evaluation of vascular permeability in the gerbil brain after transient ischemia using Evans blue fluorescence. *J Cereb Blood Flow Metab* 8(2):282-284.
- Wolburg H, Wolburg-Buchholz K, Kraus J, Rascher-Eggstein G, Liebner S, Hamm S, Duffner F, Grote EH, Risau W, Engelhardt B. 2003. Localization of claudin-3 in tight junctions of the blood-brain barrier is selectively lost during experimental autoimmune

encephalomyelitis and human glioblastoma multiforme. *Acta Neuropathol* 105(6):586-592.

Wolburg H, Wolburg-Buchholz K, Liebner S, Engelhardt B. 2001. Claudin-1, claudin-2 and claudin-11 are present in tight junctions of choroid plexus epithelium of the mouse. *Neurosci Lett* 307(2):77-80.

For Peer Review

**FIGURE LEGENDS**

**Table 1.** Table of primary antibodies used.

**Figure 1.** Microphotographs showing the distribution of vimentin and glu-tubulin immunoreactivities in coronal sections of the tuberal region of the hypothalamus. **A:** Low magnification photomontage of glu-tubulin (green) and vimentin (red) immunofluorescence. **B-D:** High magnification images showing glu-tubulin immunoreactive cilia (green, arrows) on the ventricular surface at the level of the dorsomedial nucleus of the hypothalamus (DMH) (**B, C**) and ventromedial nucleus of the hypothalamus (VMH) (**D**). Note that glu-tubulin immunoreactivity is absent in vimentin-labeled tanycytes of the arcuate nucleus of the hypothalamus (ARH) (**E**) and median eminence (**A**). Sections are counterstained using Hoechst (blue) to visualize cell nuclei and identify the morphological limits of each hypothalamic structure. 3V, third ventricle. Scale bar = 100 $\mu$ m in **A**; 20 $\mu$ m in **E**.

**Figure 2.** Microphotographs showing von Willebrand factor, MECA 32 and vimentin immunoreactivities in coronal sections of the tuberal region of the hypothalamus. **A:** Low magnification photomontage of von Willebrand factor (green) and MECA 32 (blue) immunoreactivities. **B:** Low-magnification photomontage of the same section showing vimentin immunoreactivity (red) merged with **A**. As shown in **B**, vimentin is an intermediary filament protein of the cytoskeleton that is expressed in both brain vessels and cells lining the third ventricle, including tanycytes (characterized by their elongated body and long basal process) and “typical” ependymal cells (cuboidal cells without processes located in the dorsal part of the third ventricle). **C:** High magnification image showing the vimentin-labeled processes of dorsal tanycytes (red, empty arrows) contacting von Willebrand factor-positive brain vessels (green, arrow). **D:** High magnification image showing the vimentin-labeled processes of median eminence tanycytes (red, empty arrows) contacting MECA 32-positive

pituitary portal vessels (blue, asterisk). 3V, third ventricle; ME, median eminence. Scale bar = 100 $\mu$ m in **B**; 20 $\mu$ m in **C** and **D**.

**Figure 3.** Microphotographs showing the distribution of *Zonula occludens-1* (ZO-1) and vimentin immunoreactivities in coronal sections of the tuberal region of the hypothalamus. Images were acquired either at low (**B**) or high (**A**, **C**, **D-G**) magnifications. ZO-1 (green) immunoreactivity is readily visualized in capillaries of the cerebral parenchyma, which are known to display well-differentiated tight junction complexes (**A**). ZO-1-immunoreactivity is also evident at the wall of the third ventricle (**B**). Notably, ZO-1 immunostaining displays a honeycomb distribution in cuboidal ependymal cells (**C**). Ventral to the DMH, where the tanycytes appear, the honeycomb ZO-1-immunoreactive pattern gradually disappears and is replaced by an unorganized staining pattern (**D**). This unorganized distribution of ZO-1-immunoreactivity becomes obvious in the tanycytes of the ARH (**E**). In contrast, tanycytes of the median eminence exhibit a honeycomb pattern of ZO-1 expression (**F,G**). Sections are counterstained using Hoechst (blue) to visualize cell nuclei and recognize the morphological limits of each hypothalamic structure. 3V, third ventricle; ARH, arcuate nucleus of the hypothalamus; DMH, dorsomedial nucleus of the hypothalamus; VMH, ventromedial nucleus of the hypothalamus. Scale bar = 100 $\mu$ m in **B**; 20 $\mu$ m in **G**.

**Figure 4.** Microphotographs showing the distribution of occludin and vimentin immunoreactivities in coronal sections of the tuberal region of the hypothalamus. Images were acquired either at low (**B**) or high (**A**, **C**, **D-G**) magnifications. Occludin (green) immunoreactivity is readily visualized in capillaries of the cerebral parenchyma, which are known to display well-differentiated tight junction complexes (**A**). Occludin-immunoreactivity is also evident at the wall of the third ventricle (**B**). Notably, occludin immunostaining displays a honeycomb pattern of distribution in cuboidal ependymal cells (**C**). Ventral to the DMH, where tanycytes appear, the occludin-immunoreactive honeycomb

pattern gradually disappears and is replaced by an unorganized staining (**D**). This unorganized pattern of occludin-immunoreactivity becomes obvious in tanycytes of the ARH (**E**). In contrast, tanycytes of the median eminence exhibit a honeycomb expression pattern for occludin (**F,G**). Sections are counterstained using Hoechst (blue) to visualize cell nuclei and identify the morphological limits of each hypothalamic structure. 3V, third ventricle; ARH, arcuate nucleus of the hypothalamus; DMH, dorsomedial nucleus of the hypothalamus; VMH, ventromedial nucleus of the hypothalamus. Scale bar = 100 $\mu$ m in **B**; 20 $\mu$ m in **G**.

**Figure 5.** Confocal images showing two different expression patterns for occludin. **A**: Overlay and maximum projection of the z-stack files of a color-combined image, demonstrating the unorganized distribution of occludin (green) in tanycytes lining the arcuate nucleus (vimentin, red). Nuclei are counterstained using Hoechst (blue). **B**: Three-dimensional representation of **A** obtained with the Imaris 6.0 software. **C**: Overlay and maximum projection of the z-stack files of a color-combined image showing the honeycomb pattern of expression for occludin (green) in tanycytes of the median eminence (vimentin, red). Nuclei are counterstained using hoechst (blue) **D**: Three-dimensional representation of **C** obtained with the Imaris 6.0 software. 3V, third ventricle; ARH, arcuate nucleus of the hypothalamus; ME, median eminence. Scale bar = 20 $\mu$ m in **C**.

**Figure 6.** Microphotographs showing the distribution of occludin immunoreactivity in sagittal sections of the tuberal region of the hypothalamus. **A**: Low magnification photomontage of Hoechst fluorescence showing the different brain structures. **B-D**: High magnification images showing the honeycomb pattern of occludin-immunoreactivity (green) in cuboidal ependymal cells (**B**) and tanycytes of the median eminence (**C**), whereas tanycytes of the arcuate nucleus display an unorganized pattern of immunoreactivity for occludin (**D**). 3V, third ventricle; OCh, Optic Chiasma; ME, median eminence; Pit, pituitary gland. Scale bar = 500 $\mu$ m in **A**; 20 $\mu$ m in **D**.

**Figure 7.** Morphological identification of the different ependymal cell types. **A-D:** Microphotographs showing the pattern of vimentin immunostaining (red) at the level of the ME (A), ARH (B), VMH (C) and DMH (D). **E-H:** Microphotographs showing the pattern of occludin immunostaining (green) at the level of the ME (E), ARH (F), VMH (G) and DMH (H). **I:** Merged picture of A and E. **J:** Merged picture of B and F. **K:** Merged picture of C and G. **L:** Merged picture of D and H. The three cell types identified on the ventricular surface of the third ventricle were tanycytes harboring a honeycomb pattern of occludin (empty arrows), tanycytes harboring an unorganized pattern of occludin (arrows) and cuboidal ependymal cells harboring a honeycomb pattern of occludin (empty arrowheads). The nuclei are counterstained using Hoechst (blue). **M:** Quantification of the basic cell types found on the ventricular surface at the ME, ARH, VMH and DMH zones. ARH, arcuate nucleus of the hypothalamus; DMH, dorsomedial nucleus of the hypothalamus; ME, median eminence; VMH, ventromedial nucleus of the hypothalamus. Scale bar = 20 $\mu$ m in **L**.

**Figure 8.** Microphotographs showing the distribution of claudin 5 and vimentin immunoreactivities in coronal sections of the tuberal region of the hypothalamus. **A-B:** Images showing the honeycomb pattern of immunoreactivity for claudin 5 (green) in both cuboidal ependymal cells (vimentin, red) (A) and tanycytes of the median eminence (vimentin, red) (B). **C:** Image showing the unorganized pattern of immunoreactivity for claudin 5 in tanycytes of the arcuate nucleus. Sections are counterstained using Hoechst (blue) to visualize cell nuclei and recognize the morphological limits of each hypothalamic structure. 3V, third ventricle. Scale bar = 20 $\mu$ m in **C**.

**Figure 9.** Microphotographs showing the distribution of claudin 3 immunoreactivity in coronal sections of the tuberal region of the hypothalamus. **A:** Low magnification photomontage of claudin 3 immunoreactivity (green). **B-D:** High magnification photomontages showing that claudin 3 is expressed in brain capillaries (B) but not in the

ependymal layer of the wall of the 3V (**C,D**). Sections are counterstained using Hoechst (blue) to visualize cell nuclei and recognize the morphological limits of each hypothalamic structure. Scale bar = 100 $\mu$ m in **A**, 20 $\mu$ m in **D**.

**Figure 10.** Microphotographs showing the distribution of claudin 1 and vimentin immunoreactivities in coronal sections of the tuberal region of the hypothalamus. Images were acquired either at low (**A**) or high (**B,C**) magnifications. **A:** Photomontage showing claudin 1-immunoreactivity (green) in tanycytes of the median eminence (vimentin positive cells with processes, red). **B:** Photomontage showing the transition zone between arcuate tanycytes that do not express claudin 1 (empty arrowhead) and tanycytes of the median eminence that exhibit a honeycomb pattern of immunoreactivity for claudin 1 (green, empty arrow). **C:** High magnification image showing claudin 1 immunoreactivity in ventral tanycytes of the median eminence (green, empty arrow). Sections are counterstained using Hoechst (blue) to visualize cell nuclei and recognize the morphological limits of each hypothalamic structure. 3V, third ventricle. Scale bar = 100 $\mu$ m in **A**; 20 $\mu$ m in **B** and **C**.

**Figure 11.** Occludin immunoreactivity correlated with the permeability of Evans blue at the tuberal region of the hypothalamus. **A:** Low magnification photomontage showing fluorescence after intravenous injection of Evans blue dye (grey). **B:** Low magnification photomontage of the same section showing occludin (tight junction protein, green) and MECA 32 (fenestrated capillary marker, red) immunoreactivities. Occludin (green) is expressed by all cells surrounding the third ventricle but the pattern of expression is not uniform. **C-E:** High magnification images captured from the same section. Cuboidal ependymal cells (**C**) and tanycytes at the level of the median eminence (**E**) display a honeycomb pattern of expression for occludin (green, empty arrows). Tanycytes at the level of the arcuate nucleus exhibit an unorganized pattern of expression for occludin (green, empty arrowhead, **D**). **F:** Color-combined image of **A** and **B**. When injected into the blood, the dye is

stopped by tight junctions of the blood-brain barrier, and is confined into brain vessels that are immunoreactive for occludin (green, arrows). By contrast, the dye reaches the median eminence parenchyma through the fenestrated portal vessels that are immunoreactive for MECA 32 (red, asterisks). **G**: Low magnification photomontage showing fluorescence after intracerebroventricular injection of Evans blue dye (grey). **H**: Low magnification photomontage of the same section showing occludin (green) and MECA 32 (red) immunoreactivities. **I-K**: High magnification images captured from the same section showing the honeycomb pattern of expression for occludin in cuboidal ependymal cells (green, empty arrow) (**I**) and tanycytes of the median eminence (green, empty arrow) (**K**) and the unorganized pattern of expression for occludin in tanycytes lining the arcuate nucleus (green, empty arrowhead) (**J**). **L**: Color-combined image of **G** and **H**. When injected into the cerebrospinal fluid, Evans blue diffusion is restricted to the arcuate nucleus and is found to diffuse neither into other hypothalamic nuclei nor into the median eminence. The honeycomb pattern of occludin expression corresponds to the non-diffusion of the dye, whereas the unorganized pattern of expression for occludin may be associated with diffusion of the dye into the arcuate nucleus. Sections are counterstained using Hoechst (blue) to visualize cell nuclei and recognize the morphological limits of each hypothalamic structure. 3V, third ventricle; ARH, arcuate nucleus of the hypothalamus. Scale bar = 20 $\mu$ m in **E** and **K**; 100 $\mu$ m in **F** and **L**.

**Figure 12.** Representative drawing summarizing the distribution of tight junction proteins in the tuberal region of the hypothalamus. 3V, third ventricle; ARH, arcuate nucleus of the hypothalamus; DMH, dorsomedial nucleus of the hypothalamus; ME, median eminence; VMH, ventromedial nucleus of the hypothalamus.

Antigen	Immunogen	Manufacturer, species, type, catalog number	Dilution used
occludin	GST fusion protein consisting of aa 372-522 from C-terminus of human occludin fused to GST	Zymed (San Francisco, CA), rabbit polyclonal, #1379345	1:500
zonula occludens-1	69 kD fusion protein corresponding to aa 463-1109 of human ZO-1	Zymed, rabbit polyclonal, #60303915	1:500
claudin 1	N-CRK TTS YPT PRP YPK PAP SSG KDY V- C synthetic peptide in the C-terminal sequence of human claudin 1	Zymed, rabbit polyclonal, #60782673	1:100
claudin 3	N-CPR STG PGT GTG TAY DRK DYV-C synthetic peptide in the C-terminal sequence of human claudin 3	Zymed, rabbit polyclonal, #1376469	1:100
claudin 5	N- CYS APR RPT ANG DYD KKN YV – C synthetic peptide in the C-terminal sequence of mouse claudin 5	Zymed, rabbit polyclonal, #51001292	1:100
detyrosinated tubulin	N-GEEEGEE-C synthetic peptide corresponding to the seven C-terminal aa	Chemicon (Temecula, CA), rabbit polyclonal, #LV1422976	1:500
vimentin	recombinant Syrian gold hamster vimentin	Chemicon, chicken polyclonal, #0604026541	1:2,000
von Willebrand factor	von Willebrand factor purified from human plasma	Sigma (Saint Quentin Fallavier, France), rabbit polyclonal	1:200
MECA 32	murine lymph node stroma	Gift from Pr Britta Engelhardt (Switzerland), rat monoclonal	1:200

Table 1

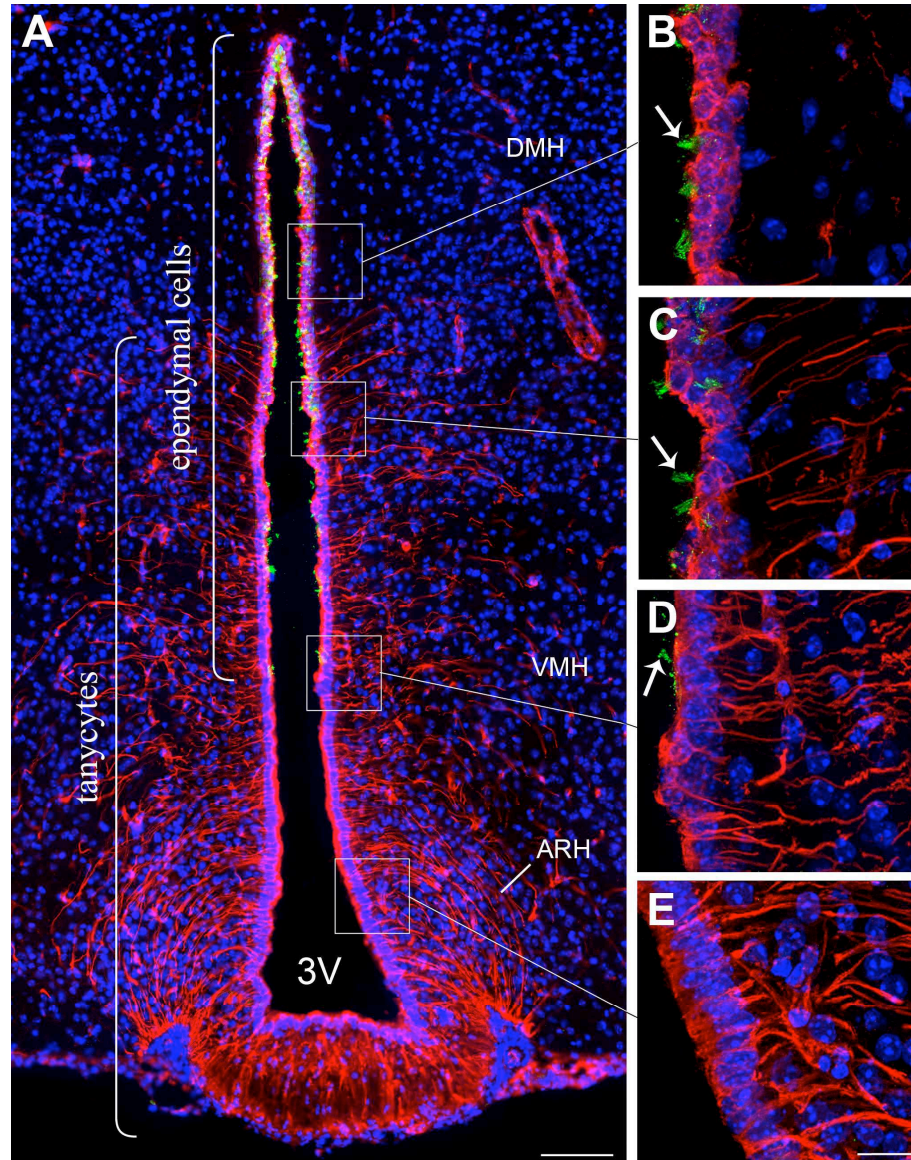


Figure 1

Microphotographs showing the distribution of vimentin and glu-tubulin immunoreactivities in coronal sections of the tuberal region of the hypothalamus. A: Low magnification photomontage of glu-tubulin (green) and vimentin (red) immunofluorescence. B-D: High magnification images showing glu-tubulin immunoreactive cilia (green, arrows) on the ventricular surface at the level of the dorsomedial nucleus of the hypothalamus (DMH) (B, C) and ventromedial nucleus of the hypothalamus (VMH) (D). Note that glu-tubulin immunoreactivity is absent in vimentin-labeled tanyocytes of the arcuate nucleus of the hypothalamus (ARH) (E) and median eminence (A). Sections are counterstained using Hoechst (blue) to visualize cell nuclei and identify the morphological limits of each hypothalamic structure. 3V, third ventricle. Scale bar = 100 $\mu$ m in A; 20 $\mu$ m in E. 172x228mm (300 x 300 DPI)

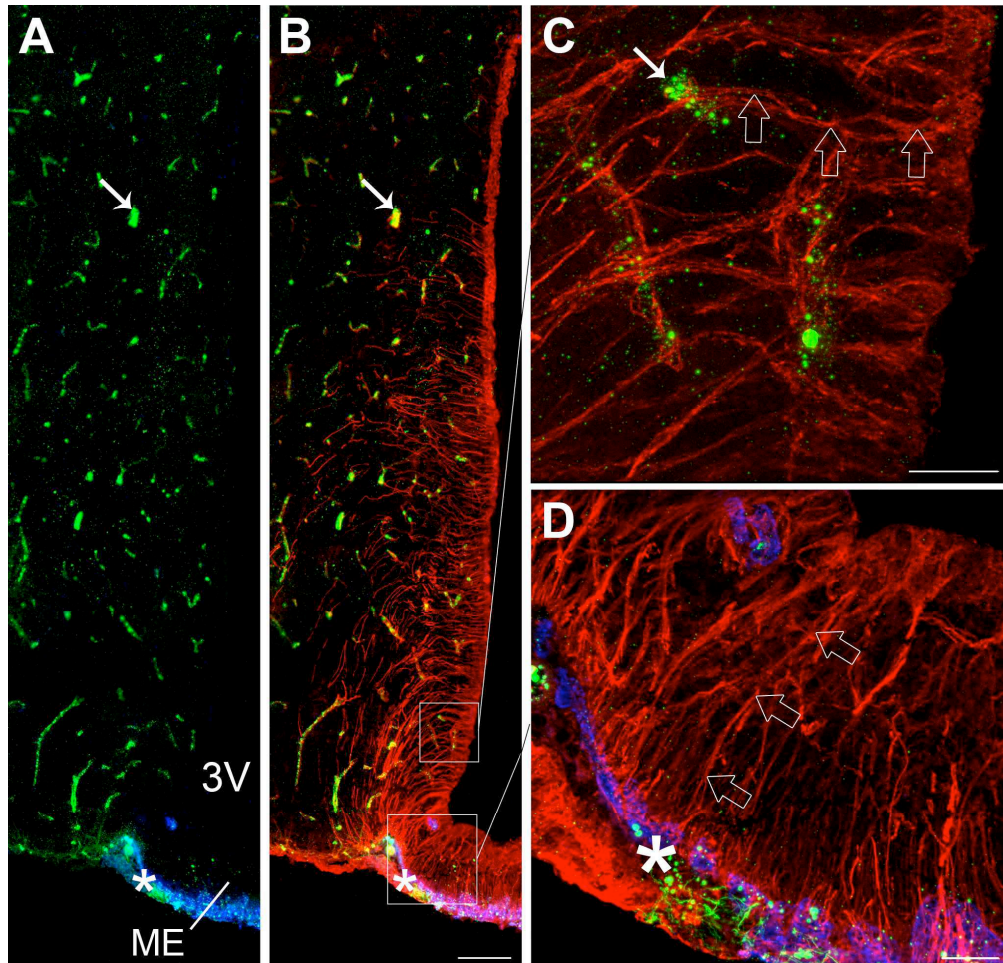


Figure 2

Microphotographs showing von Willebrand factor, MECA 32 and vimentin immunoreactivities in coronal sections of the tuberal region of the hypothalamus. A: Low magnification photomontage of von Willebrand factor (green) and MECA 32 (blue) immunoreactivities. B: Low-magnification photomontage of the same section showing vimentin immunoreactivity (red) merged with A. As shown in B, vimentin is an intermediary filament protein of the cytoskeleton that is expressed in both brain vessels and cells lining the third ventricle, including tanocytes (characterized by their elongated body and long basal process) and "typical" ependymal cells (cuboidal cells without processes located in the dorsal part of the third ventricle). C: High magnification image showing the vimentin-labeled processes of dorsal tanocytes (red, empty arrows) contacting von Willebrand factor-positive brain vessels (green, arrow). D: High magnification image showing the vimentin-labeled processes of median eminence tanocytes (red, empty arrows) contacting MECA 32-positive pituitary portal vessels (blue, asterisk). 3V, third ventricle; ME, median eminence. Scale bar = 100 $\mu$ m in B; 20 $\mu$ m in C and D. 172x174mm (300 x 300 DPI)

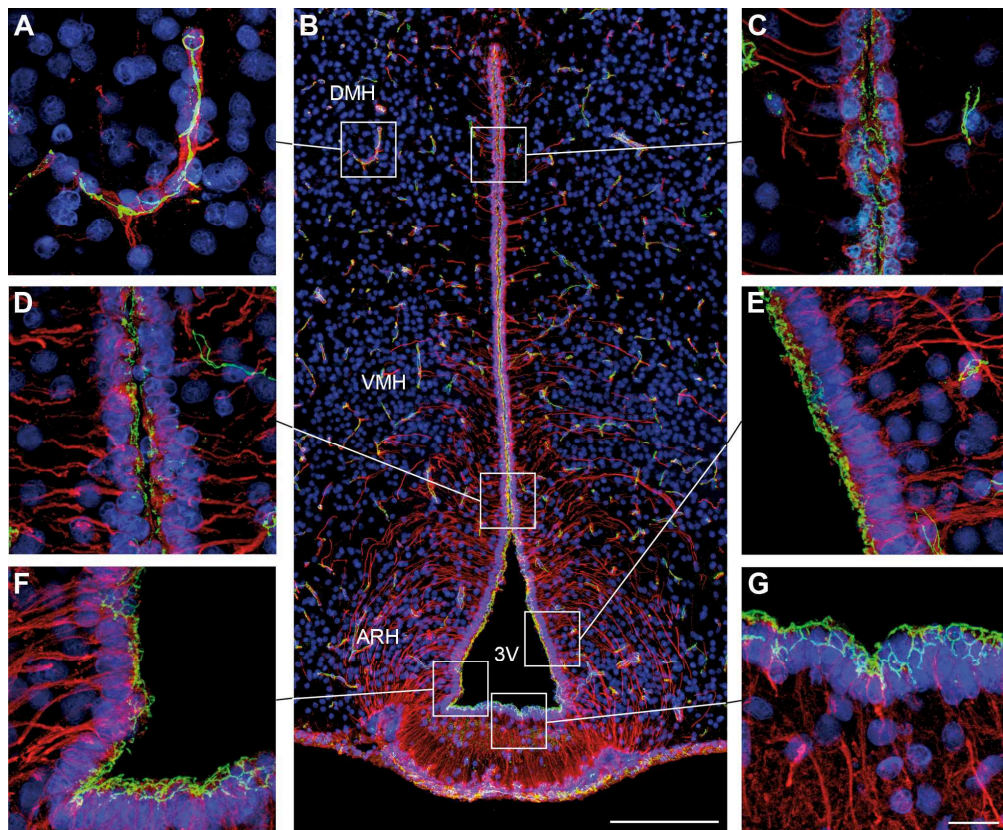


Figure 3

Microphotographs showing the distribution of Zonula occludens-1 (ZO-1) and vimentin immunoreactivities in coronal sections of the tuberal region of the hypothalamus. Images were acquired either at low (B) or high (A, C, D-G) magnifications. ZO-1 (green) immunoreactivity is readily visualized in capillaries of the cerebral parenchyma, which are known to display well-differentiated tight junction complexes (A). ZO-1-immunoreactivity is also evident at the wall of the third ventricle (B). Notably, ZO-1 immunostaining displays a honeycomb distribution in cuboidal ependymal cells (C). Ventral to the DMH, where the tanycytes appear, the honeycomb ZO-1-immunoreactive pattern gradually disappears and is replaced by an unorganized staining pattern (D). This unorganized distribution of ZO-1-immunoreactivity becomes obvious in the tanycytes of the ARH (E). In contrast, tanycytes of the median eminence exhibit a honeycomb pattern of ZO-1 expression (F,G). Sections are counterstained using Hoechst (blue) to visualize cell nuclei and recognize the morphological limits of each hypothalamic structure. 3V, third ventricle; ARH, arcuate nucleus of the hypothalamus; DMH, dorsomedial nucleus of the hypothalamus; VMH, ventromedial nucleus of the hypothalamus. Scale bar = 100 $\mu$ m in B; 20 $\mu$ m in G.

172x150mm (300 x 300 DPI)

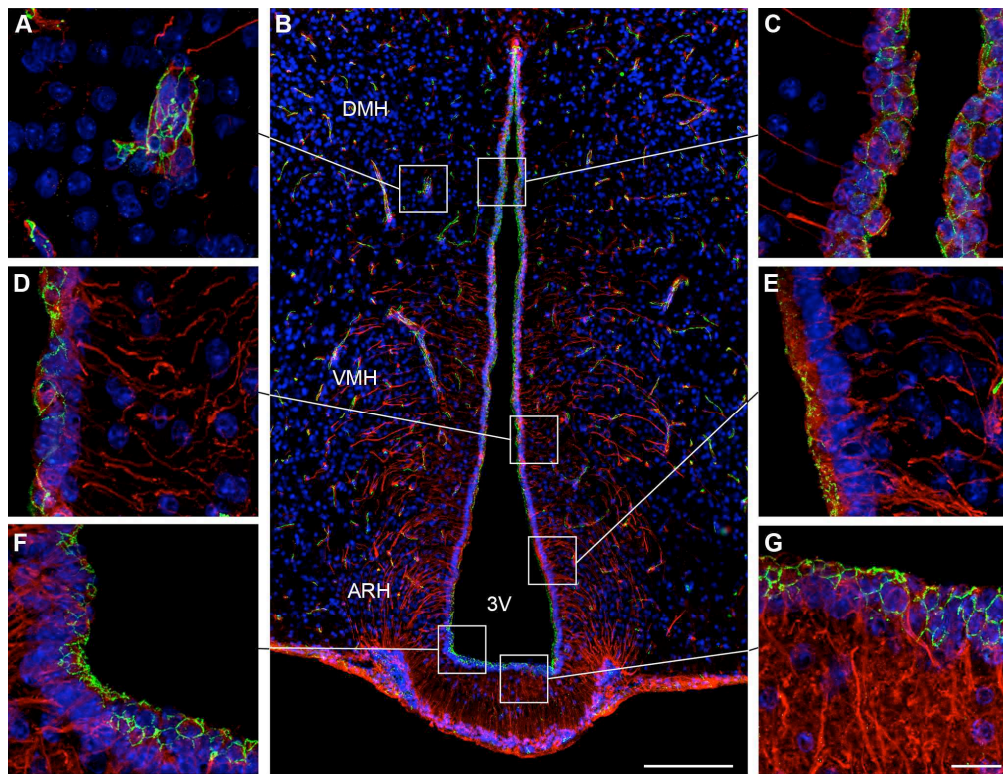


Figure 4

Microphotographs showing the distribution of occludin and vimentin immunoreactivities in coronal sections of the tuberal region of the hypothalamus. Images were acquired either at low (B) or high (A, C, D-G) magnifications. Occludin (green) immunoreactivity is readily visualized in capillaries of the cerebral parenchyma, which are known to display well-differentiated tight junction complexes

(A). Occludin-immunoreactivity is also evident at the wall of the third ventricle (B). Notably, occludin immunostaining displays a honeycomb pattern of distribution in cuboidal ependymal cells (C). Ventral to the DMH, where tanycytes appear, the occludin-immunoreactive honeycomb pattern gradually disappears and is replaced by an unorganized staining (D). This unorganized pattern of occludin-immunoreactivity becomes obvious in tanycytes of the ARH (E). In contrast, tanycytes of the median eminence exhibit a honeycomb expression pattern for occludin (F,G). Sections are counterstained using Hoechst (blue) to visualize cell nuclei and identify the morphological limits of each hypothalamic structure. 3V, third ventricle; ARH, arcuate nucleus of the hypothalamus; DMH, dorsomedial nucleus of the hypothalamus; VMH, ventromedial nucleus of the hypothalamus. Scale

bar = 100 $\mu$ m in B; 20 $\mu$ m in G.  
172x140mm (300 x 300 DPI)

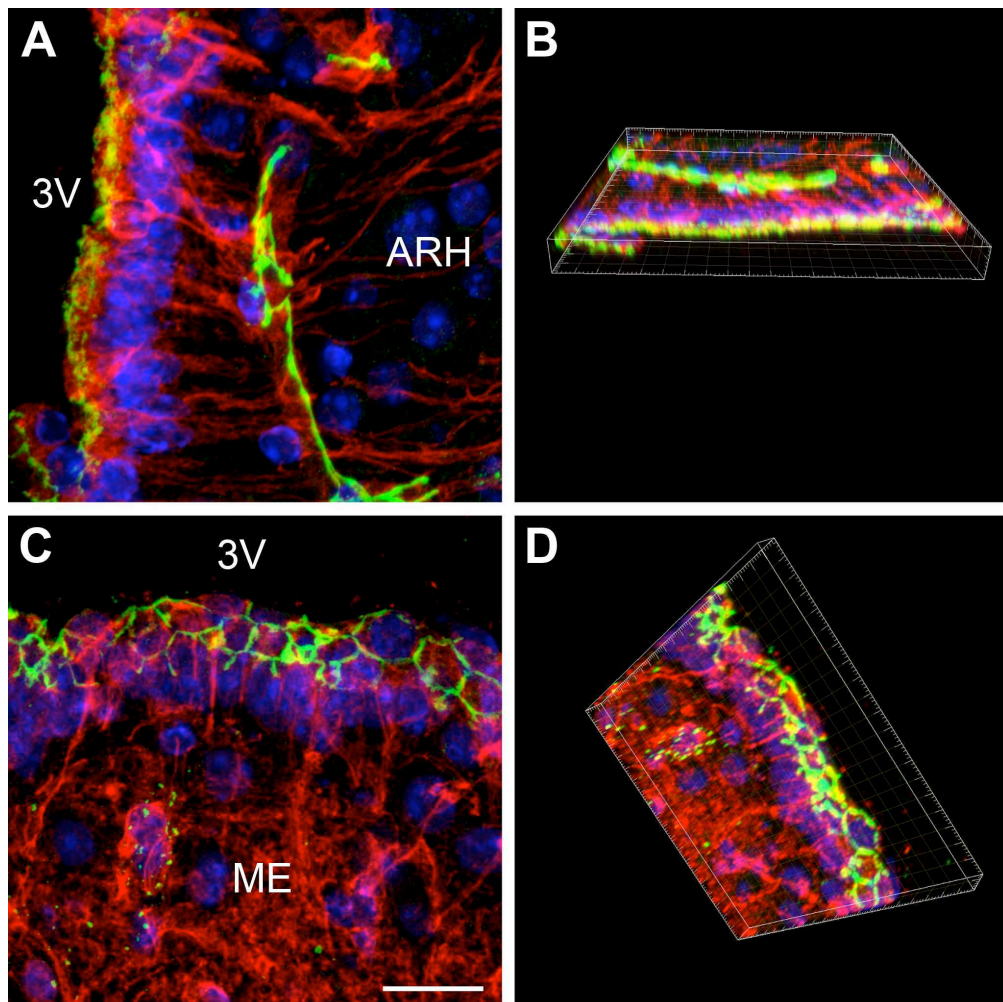


Figure 5

Confocal images showing two different expression patterns for occludin. A: Overlay and maximum projection of the z-stack files of a color-combined image, demonstrating the unorganized distribution of occludin (green) in tanycytes lining the arcuate nucleus (vimentin, red). Nuclei are counterstained using Hoechst (blue). B: Three-dimensional representation of A obtained with the Imaris 6.0 software. C: Overlay and maximum projection of the z-stack files of a color-combined image showing the honeycomb pattern of expression for occludin (green) in tanycytes of the median eminence (vimentin, red). Nuclei are counterstained using Hoechst (blue). D: Three-dimensional representation of C obtained with the Imaris 6.0 software. 3V, third ventricle; ARH, arcuate nucleus of the hypothalamus; ME, median eminence. Scale bar = 20 $\mu$ m in C. 172x182mm (300 x 300 DPI)

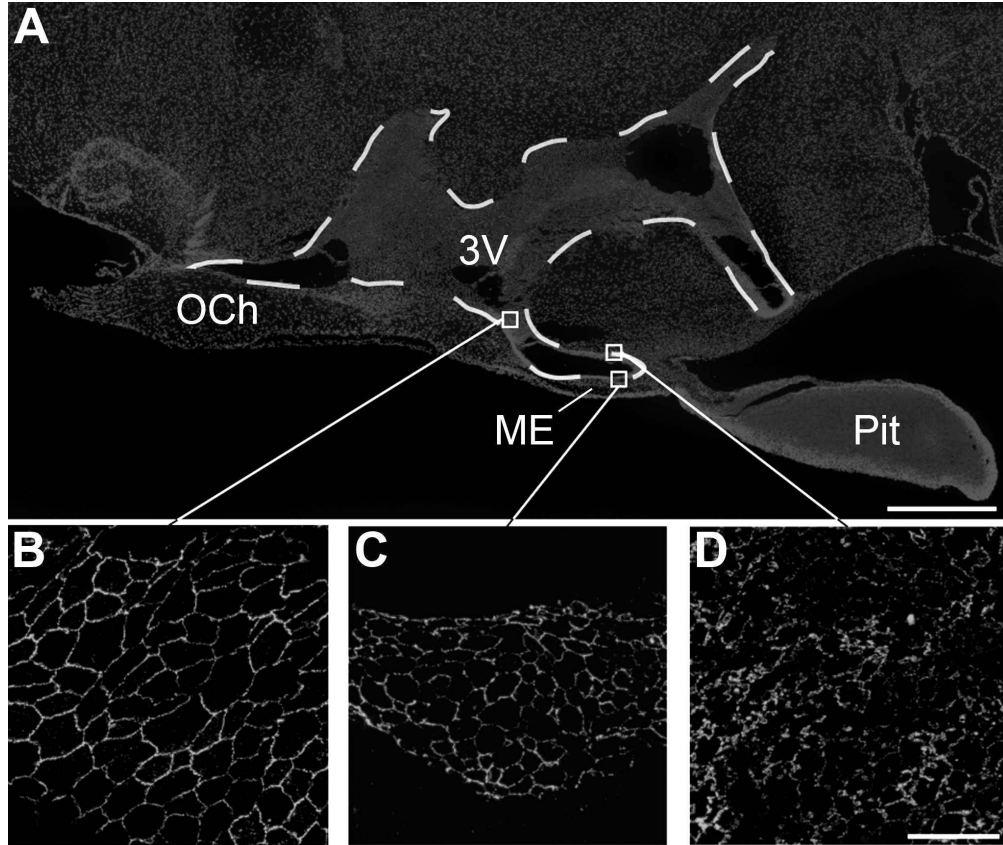


Figure 6

Microphotographs showing the distribution of occludin immunoreactivity in sagittal sections of the tuberal region of the hypothalamus. A: Low magnification photomontage of Hoechst fluorescence showing the different brain structures. B-D: High magnification images showing the honeycomb pattern of occludin-immunoreactivity in cuboidal ependymal cells (B) and tanyocytes of the median eminence (C), whereas tanyocytes of the arcuate nucleus display an unorganized pattern of immunoreactivity for occludin (D). 3V, third ventricle; OCh, Optic Chiasma; ME, median eminence; Pit, pituitary gland. Scale bar = 500 $\mu$ m in A; 20 $\mu$ m in D.  
172x160mm (300 x 300 DPI)

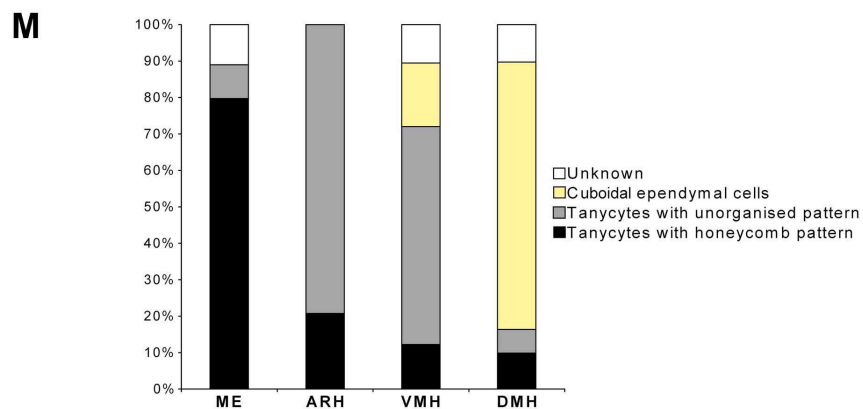
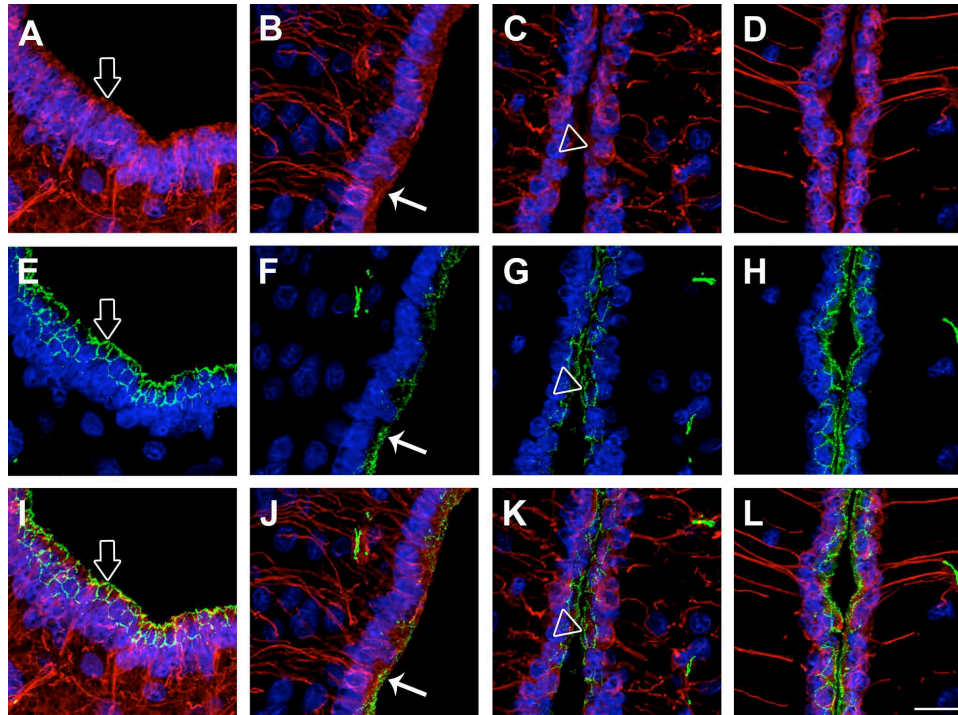


Figure 7

Morphological identification of the different ependymal cell types. A-D: Microphotographs showing the pattern of vimentin immunostaining (red) at the level of the ME (A), ARH (B), VMH (C) and DMH (D). E-H: Microphotographs showing the pattern of occludin immunostaining (green) at the level of the ME (E), ARH (F), VMH (G) and DMH (H). I: Merged picture of A and E. J: Merged picture of B and F. K: Merged picture of C and G. L: Merged picture of D and H. The three cell types identified on the ventricular surface of the third ventricle were tanycytes harboring a honeycomb pattern of occludin (empty arrows), tanycytes harboring an unorganized pattern of occludin (arrows) and cuboidal ependymal cells harboring a honeycomb pattern of occludin (empty arrowheads). The nuclei are counterstained using Hoechst (blue). M: Quantification of the basic cell types found on the ventricular surface at the ME, ARH, VMH and DMH zones. ARH, arcuate nucleus of the hypothalamus; DMH, dorsomedial nucleus of the hypothalamus; ME, median eminence; VMH, ventromedial nucleus of the hypothalamus. Scale bar = 20  $\mu$ m in L.  
172x217mm (300 x 300 DPI)

For Peer Review

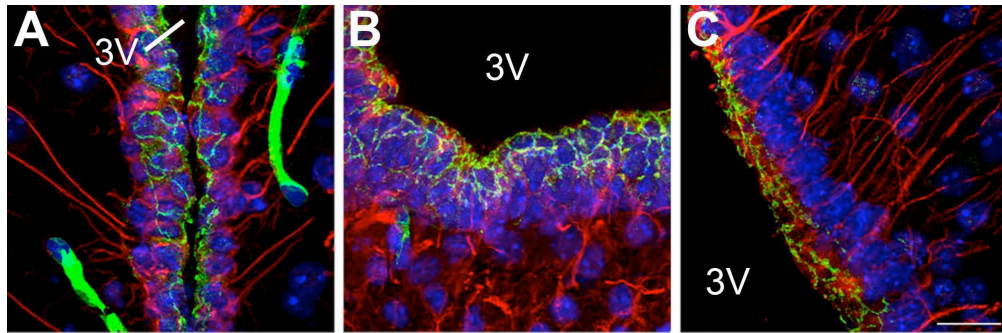


Figure 8

Microphotographs showing the distribution of claudin 5 and vimentin immunoreactivities in coronal sections of the tuberal region of the hypothalamus. A-B: Images showing the honeycomb pattern of immunoreactivity for claudin 5 (green) in both cuboidal ependymal cells (vimentin, red) (A) and tanycytes of the median eminence (vimentin, red) (B). C: Image showing the unorganized pattern of immunoreactivity for claudin 5 in tanycytes of the arcuate nucleus. Sections are counterstained using Hoechst (blue) to visualize cell nuclei and recognize the morphological limits of each hypothalamic structure. 3V, third ventricle. Scale bar = 20 $\mu$ m in C.

172x70mm (300 x 300 DPI)

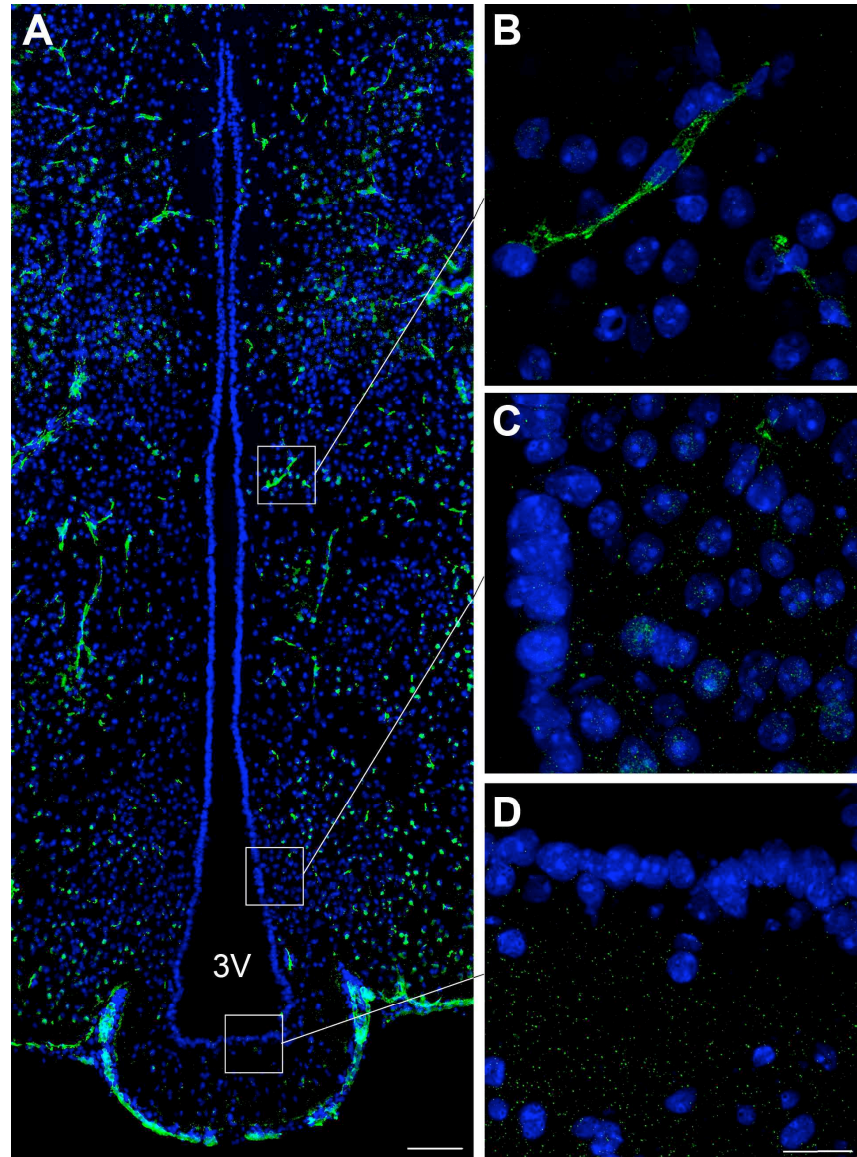


Figure 9

Microphotographs showing the distribution of claudin 3 immunoreactivity in coronal sections of the tuberal region of the hypothalamus. A: Low magnification photomontage of claudin 3 immunoreactivity (green). B-D: High magnification photomontages showing that claudin 3 is expressed in brain capillaries (B) but not in the ependymal layer of the wall of the 3V (C,D). Sections are counterstained using Hoechst (blue) to visualize cell nuclei and recognize the morphological limits of each hypothalamic structure. Scale bar = 100 $\mu$ m in A, 20 $\mu$ m in D. 163x230mm (300 x 300 DPI)

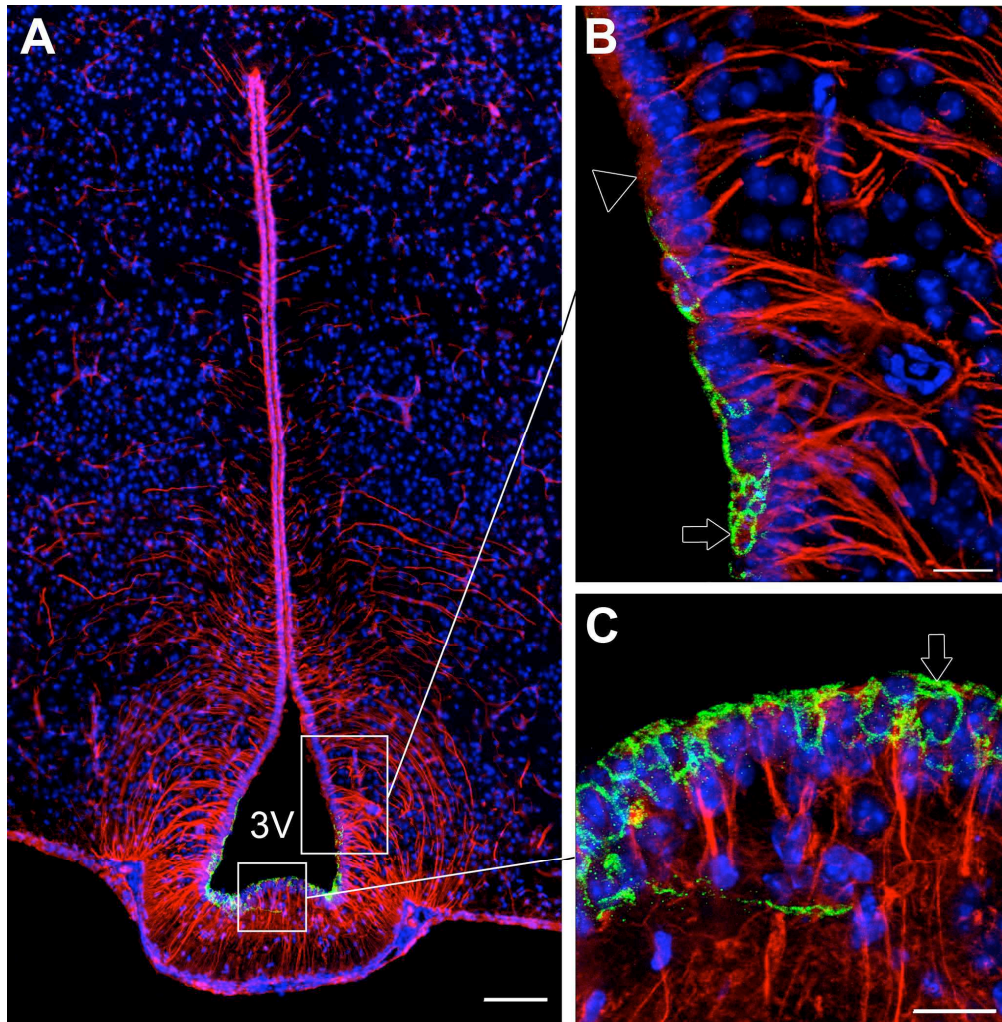


Figure 10

Microphotographs showing the distribution of claudin 1 and vimentin immunoreactivities in coronal sections of the tuberal region of the hypothalamus. Images were acquired either at low (A) or high (B,C) magnifications. A: Photomontage showing claudin 1-immunoreactivity (green) in tanyocytes of the median eminence (vimentin positive cells with processes, red). B: Photomontage showing the transition zone between arcuate tanyocytes that do not express claudin 1 (empty arrowhead) and tanyocytes of the median eminence that exhibit a honeycomb pattern of immunoreactivity for claudin 1 (green, empty arrow). C: High magnification image showing claudin 1 immunoreactivity in ventral tanyocytes of the median eminence (green, empty arrow). Sections are counterstained using Hoechst (blue) to visualize cell nuclei and recognize the morphological limits of each hypothalamic structure.

3V, third ventricle. Scale bar = 100 $\mu$ m in A; 20 $\mu$ m in B and C.

172x184mm (300 x 300 DPI)

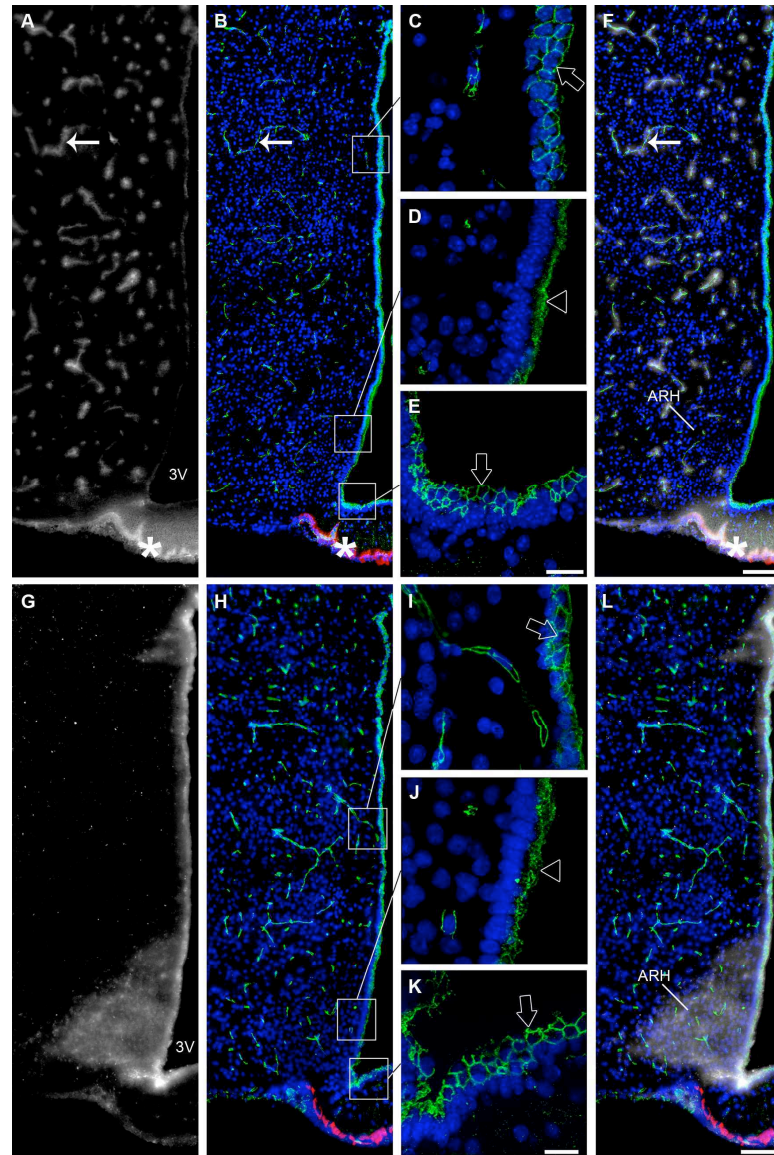


Figure 11

Occludin immunoreactivity correlated with the permeability of Evans blue at the tuberal region of the hypothalamus. A: Low magnification photomontage showing fluorescence after intravenous injection of Evans blue dye (grey). B: Low magnification photomontage of the same section showing occludin (tight junction protein, green) and MECA 32 (fenestrated capillary marker, red) immunoreactivities. Occludin (green) is expressed by all cells surrounding the third ventricle but the pattern of expression is not uniform. C-E: High magnification images captured from the same section. Cuboidal ependymal cells (C) and tanycytes at the level of the median eminence (E) display a honeycomb pattern of expression for occludin (green, empty arrows). Tanycytes at the level of the arcuate nucleus exhibit an unorganized pattern of expression for occludin (green, empty arrowhead). F: Color-combined image of A and B. When injected into the blood, the dye is stopped by tight junctions of the blood-brain barrier, and is confined into brain vessels that are immunoreactive for occludin (green, arrows). By contrast, the dye reaches the median eminence

parenchyma through the fenestrated portal vessels that are immunoreactive for MECA 32 (red, asterisks). G: Low magnification photomontage showing fluorescence after intracerebroventricular injection of Evans blue dye (grey). H: Low magnification photomontage of the same section showing occludin (green) and MECA 32 (red) immunoreactivities. I-K: High magnification images captured from the same section showing the honeycomb pattern of expression for occludin in cuboidal ependymal cells (green, empty arrow) (I) and tanycytes of the median eminence (green, empty arrow) (K) and the unorganized pattern of expression for occludin in tanycytes lining the arcuate nucleus (green, empty arrowhead) (J). L: Color-combined image of G and H. When injected into the cerebrospinal fluid, Evans blue diffusion is restricted to the arcuate nucleus and is found to diffuse neither into other hypothalamic nuclei nor into the median eminence. The honeycomb pattern of occludin expression corresponds to the non-diffusion of the dye, whereas the unorganized pattern of expression for occludin may be associated with diffusion of the dye into the arcuate nucleus.

Sections are counterstained using Hoechst (blue) to visualize cell nuclei and recognize the morphological limits of each hypothalamic structure. 3V, third ventricle; ARH, arcuate nucleus of the hypothalamus. Scale bar = 20 $\mu$ m in E and K; 100 $\mu$ m in F and L.  
147x230mm (300 x 300 DPI)

For Peer Review

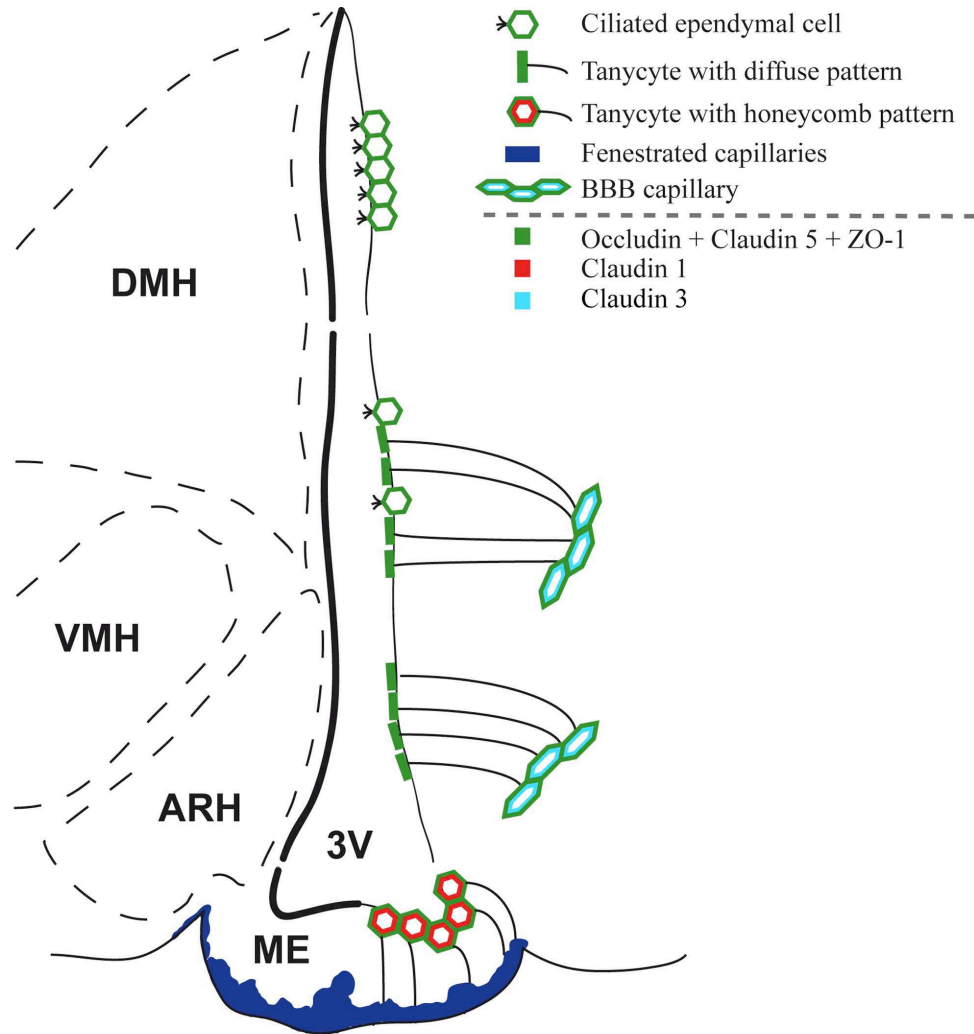
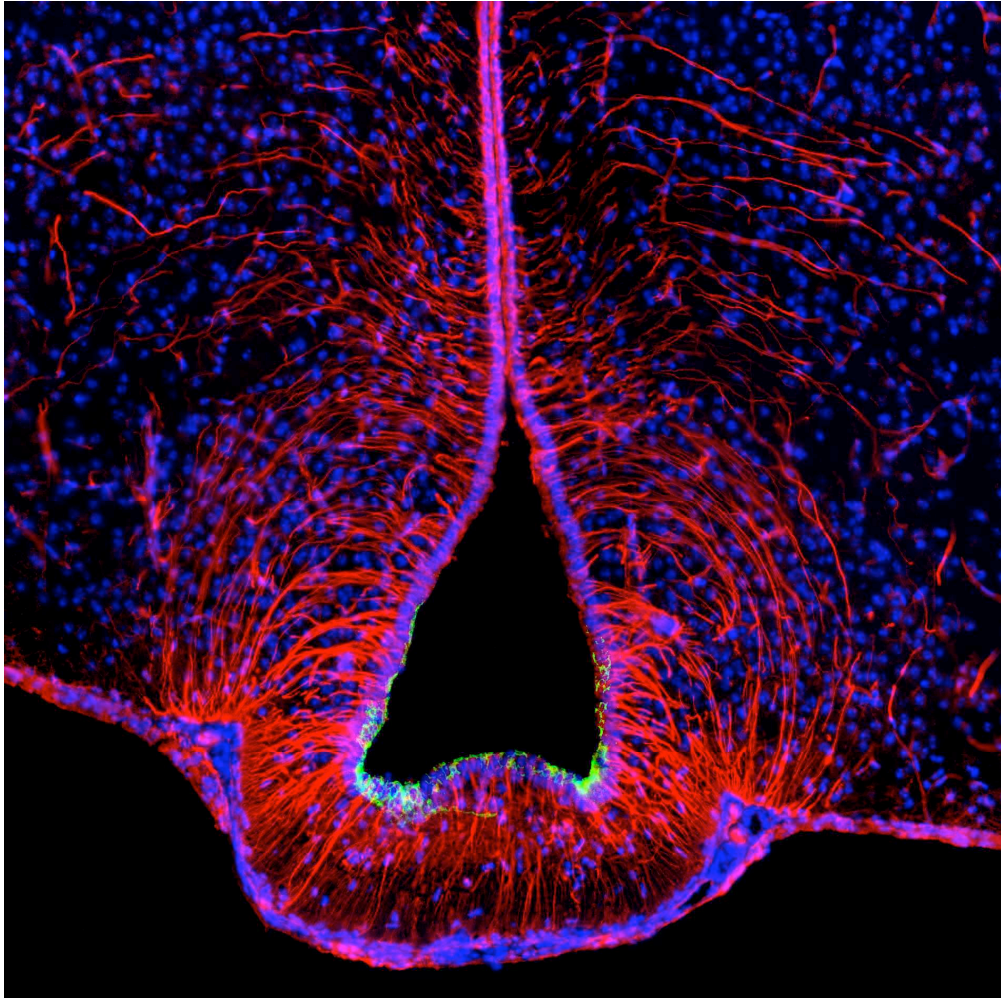


Figure 12

Representative drawing summarizing the distribution of tight junction proteins in the tuberal region of the hypothalamus. 3V, third ventricle; ARH, arcuate nucleus of the hypothalamus; DMH, dorsomedial nucleus of the hypothalamus; ME, median eminence; VMH, ventromedial nucleus of the hypothalamus.

172x186mm (300 x 300 DPI)



Cover 1. Microphotograph showing the distribution of claudin 1 (green) and vimentin (red) immunoreactivities in coronal sections of the tuberal region of the hypothalamus. Sections are counterstained using Hoechst (blue) to visualize cell nuclei and recognize the morphological limits of each hypothalamic structure.  
169x169mm (284 x 284 DPI)

**Cover.** Microphotograph showing the distribution of claudin 1 (green) and vimentin (red) immunoreactivities in coronal sections of the tuberal region of the hypothalamus. Sections are counterstained using Hoechst (blue) to visualize cell nuclei and recognize the morphological limits of each hypothalamic structure.

For Peer Review